IMPROVING TRIBOLOGICAL PROPERTIES

OF ATOMICALLY THIN GRAPHENE

WITH 1D/2D HYBRID-STRUCTURE

Ngoc-Phat Huynh

School of Mechanical Engineering

University of Ulsan, Korea

IMPROVING TRIBOLOGICAL PROPERTIES OF ATOMICALLY THIN GRAPHENE WITH 1D/2D HYBRID-STRUCTURE

Supervisor: Prof. Koo-Hyun Chung

A Dissertation

Submitted to

the Graduate School of the University of Ulsan

In partial Fulfillment of the Requirements

for the Degree of

Doctor of Philosophy

by

Ngoc-Phat Huynh

School of Mechanical Engineering

University of Ulsan, Korea

June 2022

TABLES OF CONTENTS

LISTS OF FIGURES

ABSTRACT

Two-dimensional materials, such as single and multi-layer h-BN, MoS2 and graphene, with atomic thickness and exceptional material characteristics, such as high mechanical and low friction properties making them excellent for nanoscale applications such as protective and solid lubricant coating layers. However, it was found that the coating layer might be damaged under excessive contact pressure. Therefore, fundamental understanding of tribological properties of 2D materials is crucial for further implementation of these 2D materials as protective coating layer.

In this work, a hybrid-structure of 2D and 1D materials was proposed for investigation of tribological properties. In particular, hybrid-structure of atomically thin graphene coated on CNT matrix was prepared for investigation of friction and wear properties and compare with those of graphene on SiO2 substrate. It was found that graphene on top of CNT matrix exhibited lower friction properties compare to that of graphene on SiO2 substrate. This may be due to in-plane strain which associated with partially support of CNT matrix and interaction with AFM tip during contact. In addition, low adhesion properties of graphene on CNT matrix also contribute to low friction properties of specimen. It was found that wear resistance of atomically thin graphene was enhanced with presence of CNT matrix under reciprocating scratch test. CNT matrix act as nano spring may help to reduce contact pressure so that minimize the damage of coating film. Furthermore, CNT matrix also helps to avoid the formation of pucker and hillock which may contributed by its low adhesion properties and mobility during scratch test. These characteristics assist graphene layer on CNT matrix avoid the failure primary failure mechanism of graphene and other 2D materials which associated with puckering effect.

Overall, the results of this work show positive effects of CNT matrix on tribological properties of atomically thin graphene in 1D/2D hybrid-structure. The findings were expected to provide a fundamental understanding about tribological properties of 2D and 1D/2D hybrid-structure materials so that be helpful on design of these materials at protective coating layer.

Keyworks: Graphene, CNT, hybrid-structure, atomic force microscopy, nanoscale tribology.

Chapter 1 Introduction

1.1 Background and motivation

Two-dimensional (2D) or layered materials such as hexagonal boron nitride (h-BN), molybdenum disulfide (MoS_2), and graphite are frequently used as solid lubricants in a wide range of critical engineering applications due to their low friction characteristics. It was determined that the weak interlayer bonding in the material structure was responsible for the abnormally low shear strength seen at the interaction interface of these layered materials [1, 2]. As a result of their application to the contacting surfaces of mechanical moving parts in systems, these coating layers are often used to improve tribological performance characteristics such as the reduction of friction force, the protection against wear and the resistance to surface damage.

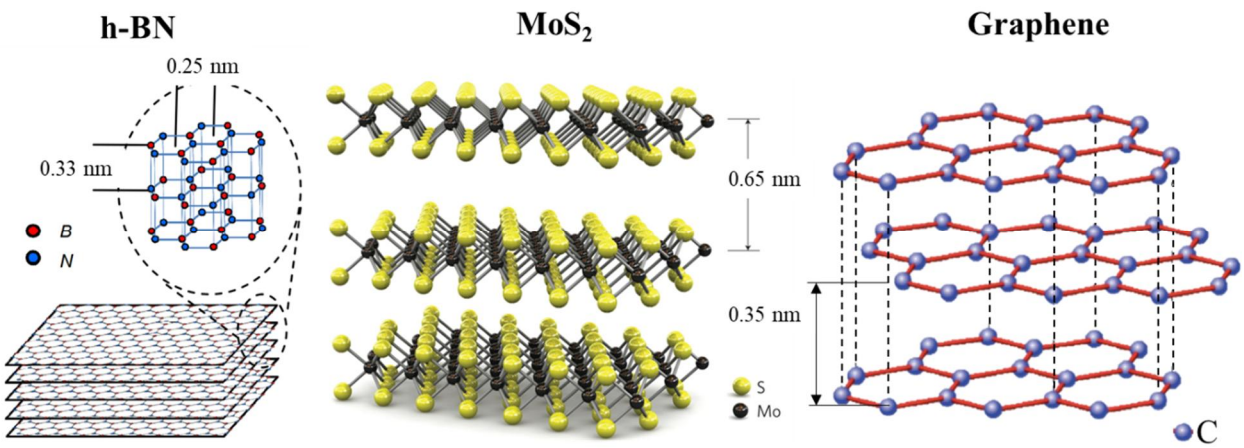

Figure 1.1 Schematic structure of atomically thin (a) h-BN[3], (b) MoS_2[4], and (c) graphene [5].

Because of their extraordinary mechanical characteristics and flexibility, atomically thin materials such as h-BN, MoS_2, and graphene continue to attract significant research [6-8]. As an example, the high elastic modulus of single layer h-BN, MoS_2, and graphene

has been reported to be around 865, 270, and 1000 GPa, respectively [8-10]. In a reciprocating scratch test, it was discovered that the coating layer of MoS_2 may be sustained after 1 million reciprocating cycles when the contact pressure is kept low, as can be seen in Figure 1.2.

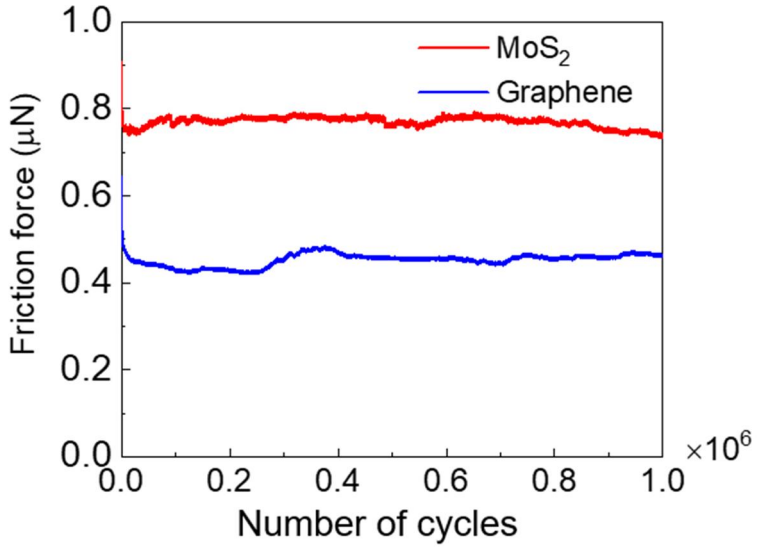

Figure 1.2 Friction force of single-layer flake after 1 million cycle of reciprocating scratch test under contact pressure as 0.80 and 0.92 GPa of MoS_2 and graphene, respectively.

It was discovered, however, that the coating layer might be destroyed when subjected to high contact pressure. For example, the critical contact pressures for single layers of h-BN, MoS_2, and graphene were determined to be around 7.57 GPa, 8.51 GPa, and 11.52 GPa, respectively [11]. In addition, the existence of a wrinkle or scratch test near the border of the coating layer might make it more likely that the coating layer will fail [12].

In this regard, it is necessary to improve the friction and wear qualities of the coating layers. Failure of the coating layer is particularly connected to contact conditions, such as contact pressure. An important reason for this study is the proposal of a novel structure, such as a hybrid-structure with 1D and 2D materials, that can assist in reducing the damage

to the coating layer when subjected to high contact pressure. In this hybrid-structure, a thin layer of 2D material was coated on 1D matrix. The 1D matrix will serve as nano springs that help to reduce the contact pressure then minimize the surface damage of coating film. In addition, the structure of 2D material on 1D matrix could also affect the friction properties which associated with mechanical properties, surface energy due to interaction inside structure. Therefore, investigation of friction and wear properties of 1D/2D hybrid-structure will be critical. Furthermore, a better knowledge of the tribological properties of 2D materials in a 1D/2D hybrid-structure can aid in the development of these materials for use as nanoscale protective and solid lubricant coating layers.

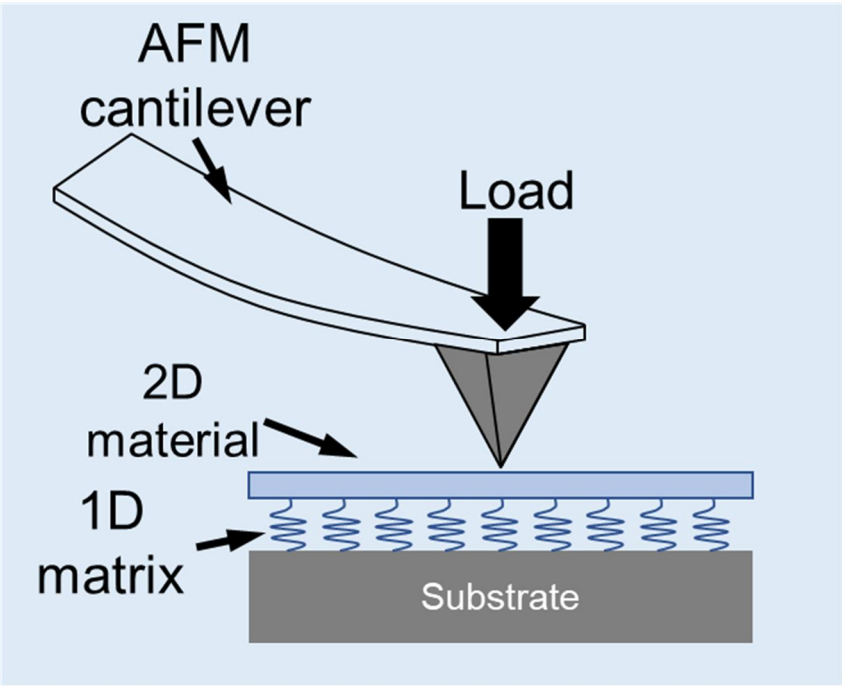

Figure 1.3 Schematic of 1D/2D hybrid-structure for investigation of friction and wear at nanoscale using AFM.

1.2 Objectives of the research

The purpose of this research is to use an atomic force microscope to investigate the friction and wear properties of a specimen consisting of a 1D/2D hybrid-structure at the nano scale. In order to accomplish this, it is essential to prepare a 1D/2D hybrid-structure specimen consisting of 2D materials layered on top of a 1D matrix. In this study, both 1D and 2D materials, specifically graphene and multi-wall carbon nanotubes, were utilized. To begin, a procedure known as mechanical exfoliation was utilized in order to produce a layer of graphene that was atomically thin. The desired graphene flake was then transferred onto a matrix of multi-wall carbon nanotubes (CNTs) that had been prepared using the spinning coating process. Several conditions were tested on the specimen, including normal force, thickness of the CNT matrix, orientation of the CNT, and thickness of the graphene flake. Under these conditions, the frictional characteristics of the specimen were analyzed and characterized. In addition to that, the reciprocating scratch test was utilized to evaluate the wear characteristics of the specimen. The findings of this work were expected to gain a fundamental understanding about tribological properties of graphene and graphene on CNT matrix so that will aid the design of these material as protective coating layer.

1.3 Organization of the research

After the introduction in this chapter, a literature review will be conducted on the topic of the mechanical and tribological strength of graphene and other 2D materials, as well as their usage as a protective coating layer, along with their surface damage at the nanoscale. In addition to this, the use of an atomic force microscope (AFM) as a tool for researching materials on a nanoscale was also brought up. Following that, the process for the production of 1D/2D hybrid structures with atomically thin graphene on CNT matrix was presented in Chapter 3. In the chapter 4, a comprehensive investigation into the friction and wear behavior of graphene on SiO_2 substrate and graphene on CNT matrix was conducted. The friction behavior of the specimen was discussed, along with the role that CNT matrix played in reducing the amount of friction experienced by graphene in 1D/2D hybrid structures. Additionally, surface damage to the specimen was inspected, presented, and a discussion of the failure mechanism was included. The outcomes of this work are discussed in Chapter 5, together with their primary conclusions and recommendations for research.

Chapter 2 Tribology study of 2D materials with AFM

2.1 Introduction of Atomic Force Microscope

Atomic force microscopy (AFM) is a type of scanning probe microscope that has been increasingly popular since the scanning tunneling microscope was first developed. Figure 2.1 illustrates the probe, which consists of a cantilever and a sharp tip, as well as the laser, photodiode detector, and piezoelectric scanner that are located underneath the sample. The sample is scanned by the tip at the end of the cantilever, which causes the cantilever to deflect either toward or away from the sample depending on the attractive or repulsive interactions that occur between the molecules of the sample and the tip. The reflection of a detection laser beam at the rear of a cantilever is used to detect the cantilever's deflection. This reflection is subsequently turned into an electrical signal by photodiodes.

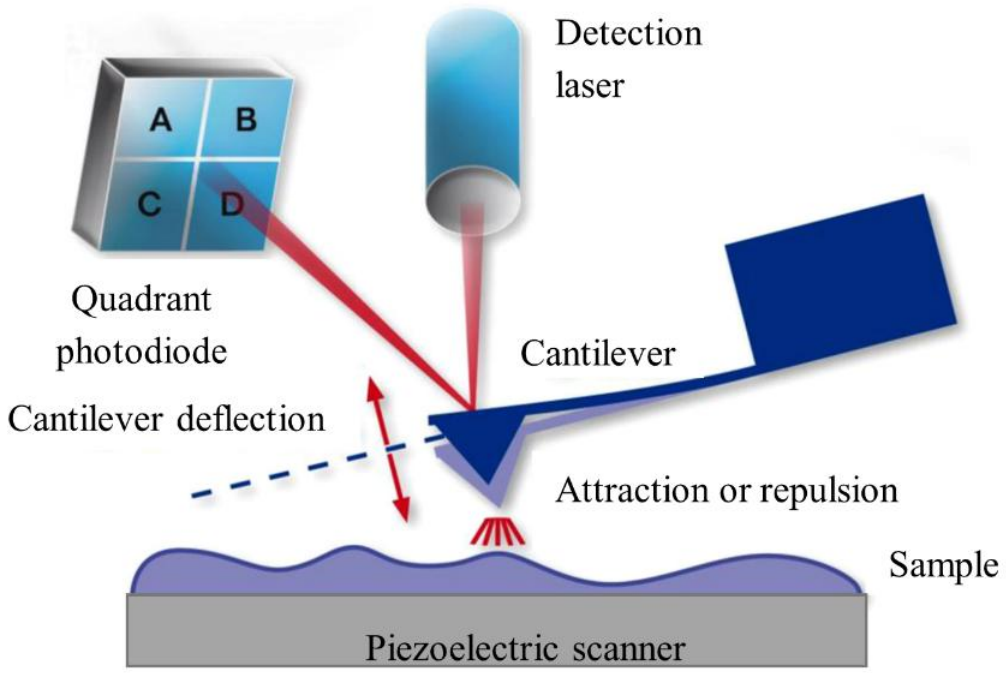

Figure 2.1 Schematic illustrating the basic principles of AFM [13]

Nanodevices can only function properly and be integrated into systems once a full understanding of surface properties at the nanoscale has been attained. The atomic force microscope (AFM) is a useful tool for doing nanoscale investigations of surface mechanical properties (such as elasticity, hardness, adhesion, and friction) as well as surface topography and structure [14-16]. In most cases, the force–indentation curve is derived from the force–displacement curve and is interpreted with the help of an appropriate contact model in order to determine the mechanical properties of the specimen [15]. A force–indentation curve illustrates the deformation of a target specimen with respect to an applied force.

Figure 2.2 displays an illustration of a force-deflection curve for an AFM cantilever (a). In accordance with the directions of movement, the curve can be divided in to two distinct sections: the extension curve, in which the point and the specimen get closer to one another, and the retraction curve, in which the point and the specimen get further apart from one another. It is then possible to divide the extension and retraction curves into three distinct regions: the zero line, the discontinuities, and the contact regions [17]. The output signal from the photodetector is equal to zero when there is no contact between the tip and the surface (region 1) because the tip is too far away from the surface. Cantilevers come into contact with surfaces when the gradient of the attractive force is greater than the force constant of the cantilever. This causes the cantilever to suddenly crash down onto the surface (point 2).

The tip will keep moving toward the specimen in the contact regions (regions 3 and 5) until it reaches a certain specified output value (point 4). When the tip reaches the desired location, it will begin to pull away from the surface. This will continue until the pull-off force between the tip and specimen is overcome by the force constant of the cantilever

(point 6), at which point it will return to its initial position (region 7). It is possible to convert the output-displacement curve of a photodetector into a force-displacement curve by multiplication of the photodetector's sensitivity to deflection and the spring constant of the cantilever. Figure 2.2 illustrates how the force-displacement curve can be turned into a force-indentation curve by simply subtracting the cantilever deflection from the displacement (b). The pull-off force of a specimen can also be used to determine the adhesive characteristics of the specimen, commonly known as the work of adhesion (based on a contact model). There have been a number of different approaches to mapping the mechanical characteristics of materials that are based on contact resonance [18, 19]. In addition, lateral force microscopy makes it possible to directly identify and map the frictional qualities of a material's surface topography and structure [20, 21]. This is made possible by the technique's ability to permit direct identification.

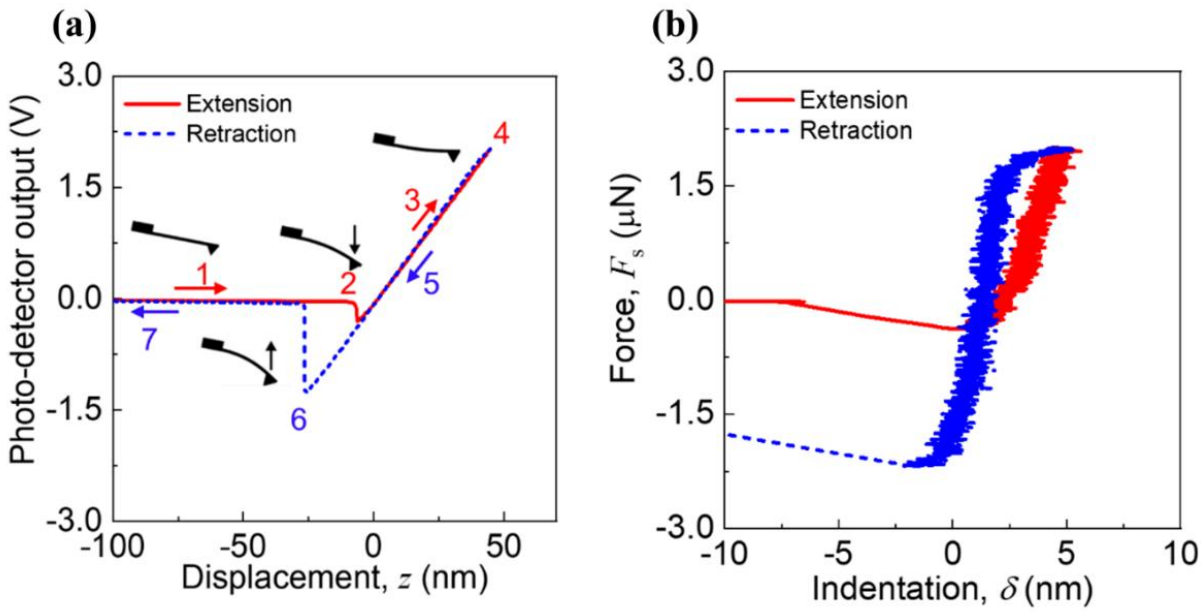

Figure 2.2 (a) An example of photo-detector output with respect to displacement of AFM cantilever during indentation and (b) corresponding force-indentation curve.

The measurement was carried out using the contact imaging mode so that the friction and wear properties of the specimen could be evaluated. The cantilever was slid across the surface of the specimen in the contact imaging mode. In addition, in order to do an accurate analysis of the cantilever's frictional qualities, the sliding direction was planned to be perpendicular to the cantilever's longitudinal axis. The cantilever was calibrated in both the normal [22] and lateral [23] directions so that quantitative force measurements could be obtained. As can be seen in Figure 2.3, the calculation for the friction force was made by taking the difference between the sliding directions of trace and retrace and dividing this by two.

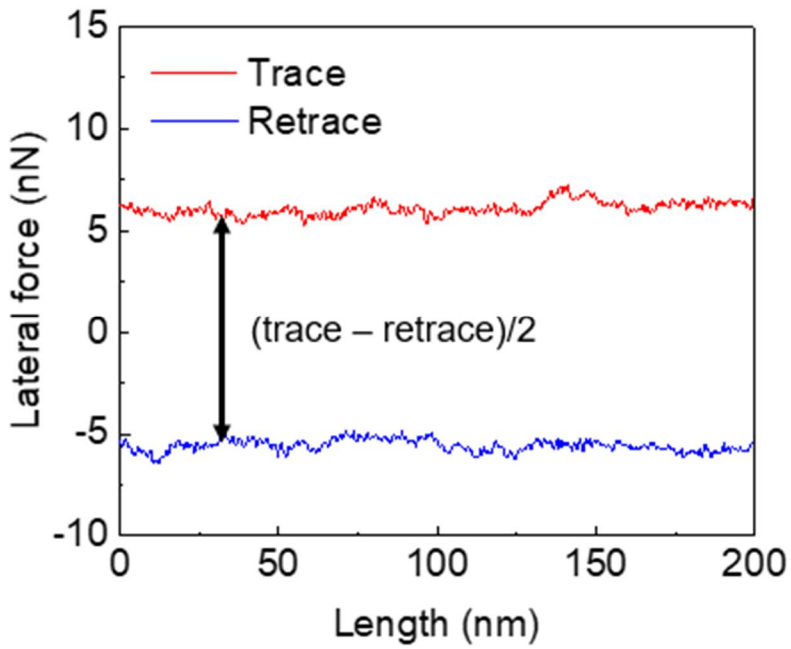

Figure 2.3 Presentative friction loop during friction force measurement.

2.2 Friction and wear properties of 2D materials

Lubrication and friction studies are generally concerned with the interactions between mechanically moving components in systems. Friction and wear are the primary causes of energy loss and significant mechanical damage. Friction and wear have a major impact on economics [24]. As a result, a detailed understanding of associated tribological processes is essential to optimize energy conservation in the majority of mechanical systems. In this regard, protective and solid lubricant coating layers have been developed to enhance the tribological properties of mechanical devices, such as surface damage resistance and friction reduction, hence extending the device's lifespan.

Two-dimensional materials, such as single and multi-layer h-BN, MoS_2 and graphene, with atomic thickness and remarkable material properties, have great potential for use as protective and permanent lubricating coatings for nano-scale devices [25]. Atomically thin materials have outstanding in-plane elastic stiffness and substantial out-plane flexibility, which makes them ideal for a variety of nanoscale applications such as protective and solid lubricant coating layers, according to the researchers. The ability of a lubricant to minimize friction and wear at a macro scale is typically determined by the development of a liquid/solid layer where the lubricant slides against itself. At the micro/nanoscale, however, that performance is most likely influenced by the surface interaction at the original interfaces [26]. As a result, a comprehensive evaluation of tribological principles at the micro- and nanoscales of these atomically thin materials is required for their applications. Extensive efforts have been made to explore the wear resistance, surface damage characteristics, and friction reduction of these atomically thin h-BN, MoS_2, and graphene to extend the lifespan of high-performance nanoscale mechanical systems.

One of the key reasons for the huge interest in using atomically thin h-BN, MoS_2, and graphene in many nanoscale applications is their extraordinary mechanical properties. Successful production of graphene via a mechanical exfoliation approach was achieved in 2004 [5]. A substantial amount of work has been put into investigating the mechanical characteristics of these atomically thin materials as a result of this discovery. Several other materials, including h-BN and MoS_2, were produced using this method, allowing for many fundamental investigations of their properties. As part of the mechanical exfoliation process, adhesive tape is used to peel the materials off from each other and onto the appropriate substrate. An atomically thin material can be deposited on a suitable substrate if the adhesion between materials is stronger than the adhesion between layers of these materials. Although mechanical exfoliation may build high-quality structures for these atomically thin materials, its low production efficiency restricts their utility to fundamental research. Intercalation-assisted exfoliation [27, 28] and liquid-based exfoliation [29, 30] are examples of mechanical exfoliation procedures that have been improved. These methods were shown to have great promise for large-scale synthesis of ultrathin materials, despite the fact that they were found to have considerable contamination in the produced products' structures.

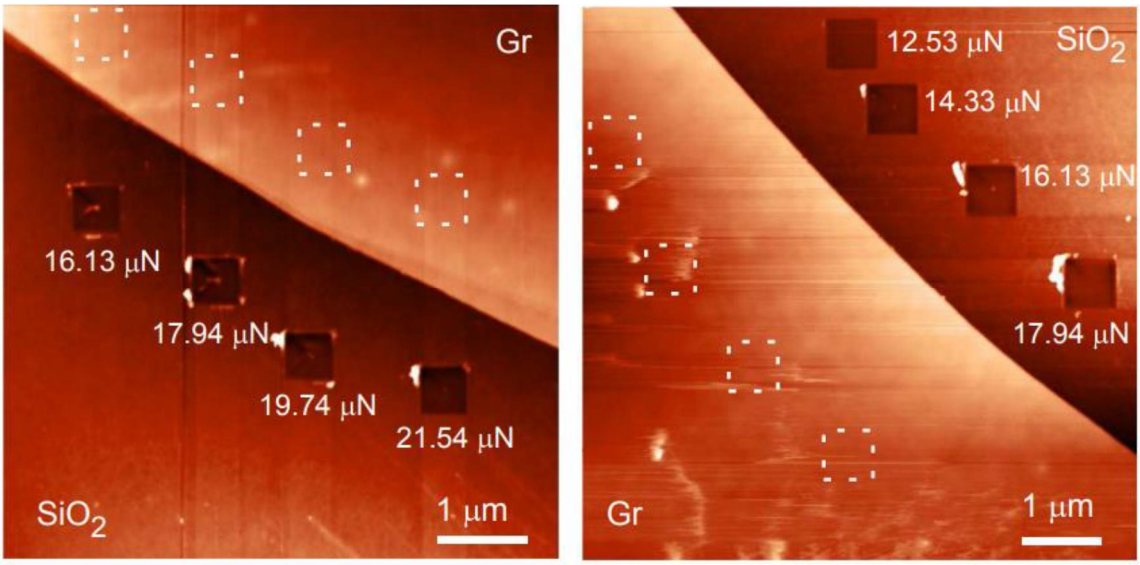

Figure 2.4 Topographic image of SiO_2 substrate and multilayer graphene (~ 4.5 nm thickness) after scratch test under various normal forces [31].

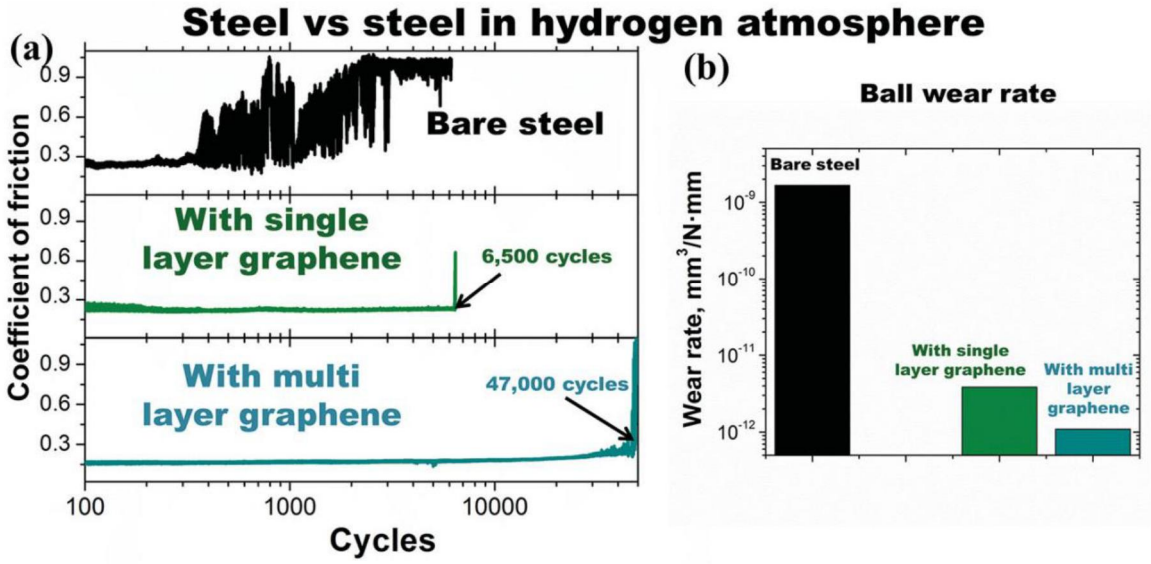

Figure 2.5 (a) Friction coefficient as function of number of cycle and (b) wear rate of steel ball slid against counter specimen with absence and absence of graphene as lubricant in hydrogen environment [32].

The tribological properties of atomically thin graphene have been extensively studied. The research has examined the wear and surface damage resistance of graphene generated

by mechanical exfoliation method [12, 31, 33], epitaxial method [33, 34], chemical vapor deposition (CVD) [32, 35-37], and thermal decomposition method [38]. Figure 2.4 shows that the multilayer graphene was likely intact after scratching under the given conditions, whereas the SiO_2 substrate was severely damaged [31]. According to Figure 2.5, at high contact pressure of 0.5 GPa, single-layer graphene could withstand 6,500 sliding cycles, whereas multi-layer graphene (3-4 layers) could survive 47,000 sliding cycles in hydrogen atmosphere[32]. The wear resistance and surface damage prevention of CVD-grown atomically thin graphene were also shown to be extremely sensitive to environmental conditions, with a far larger number of cycles sliding in hydrogen atmosphere than in nitrogen atmosphere being able to sustain CVD-grown graphene.

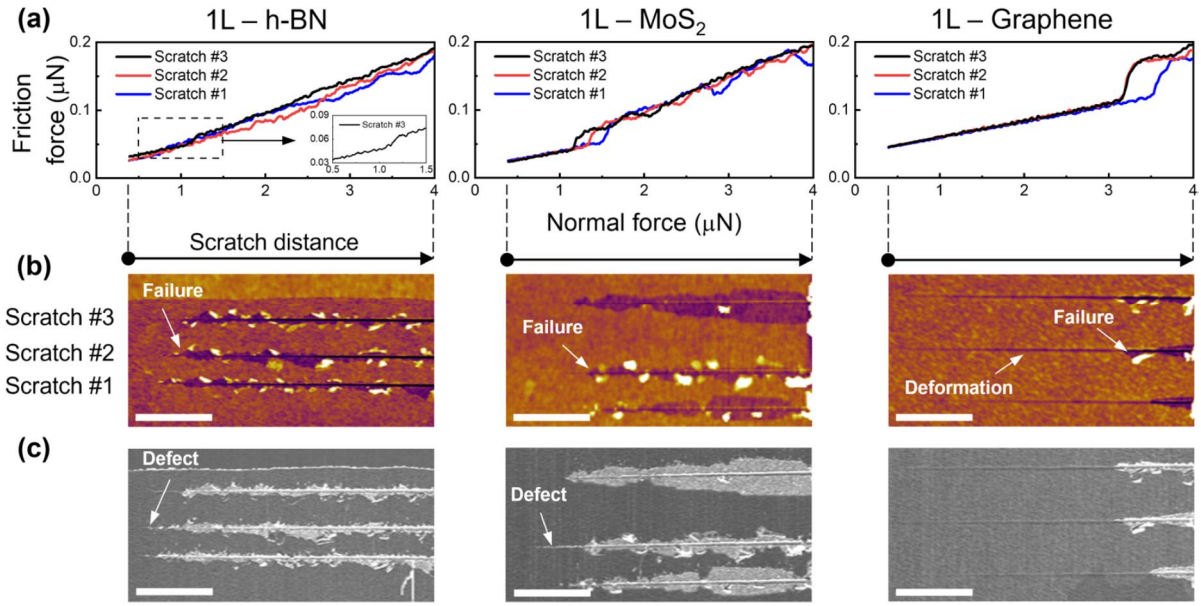

Figure 2.6 (a) Revolution of friction force during progressive scratch test of single-layer h-BN, MoS_2, and graphene and corresponding (b) Topographic image and (c) LFM image after test [11].

High shear strength may be a factor in the exceptional wear resistance of h-BN, MoS_2, and graphene. Single layer h-BN, MoS_2, and graphene have a critical contact pressure of

7.57 GPa, 8.51 GPa, and 11.52 GPa, respectively [11]. The failure of the graphene layer was demonstrated in Figure 2.7 to be connected to displacement of the underlying substrate in both experiments and computer simulation. Deformation of underlying substrates produced by an increase in normal force triggered the fracture of single-layer graphene under enough normal force [39]. Nonetheless, it is probable that the remarkable wear resistance would be detected only when the contact is placed in an internal location. Figure 2.8 shows that the graphene layer is more vulnerable when normal force is applied to the edge of the graphene flake. Furthermore, the strength of 2D materials decreases significantly when wrinkles appear on the surface. This imperfection in the graphene structure was a major factor in the graphene's failure. Defects in the structure of graphene have been shown to have an impact on its mechanical strength [40-44].

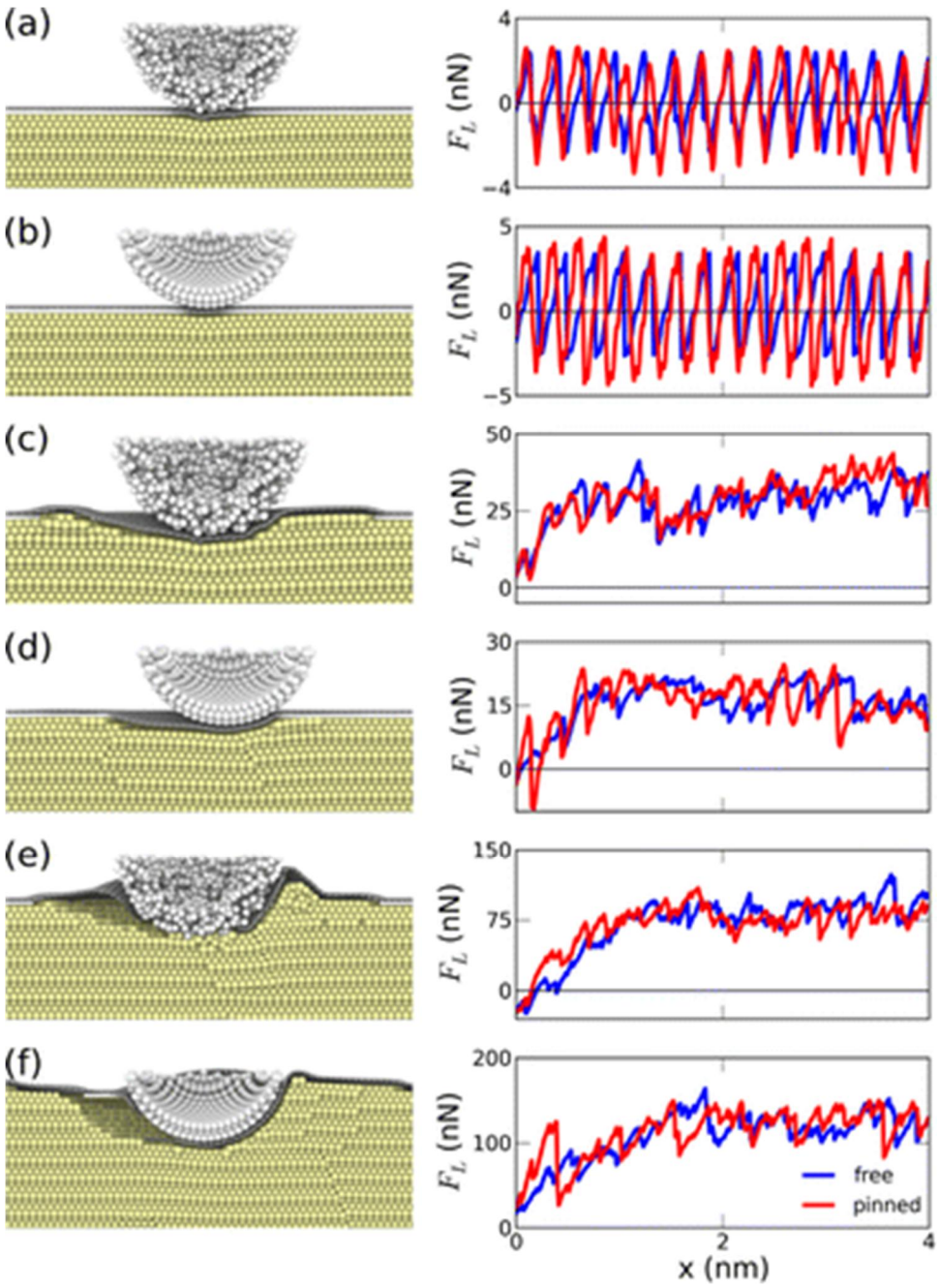

Figure 2.7 Amorphous (a,c,e) and smooth indenters were used for scratching (b,d,f). The substrates deform elastically at low normal forces F_n, while the lateral forces FL are low, resulting in clearly apparent stick–slip (a,b). The lateral pressures rise and the stick–slip pattern vanishes when the substrates deform plastically beneath the intact graphene layer (c,d). Graphene rupture results in significant plastic deformation and the development of wear tracks (e,f) [39].

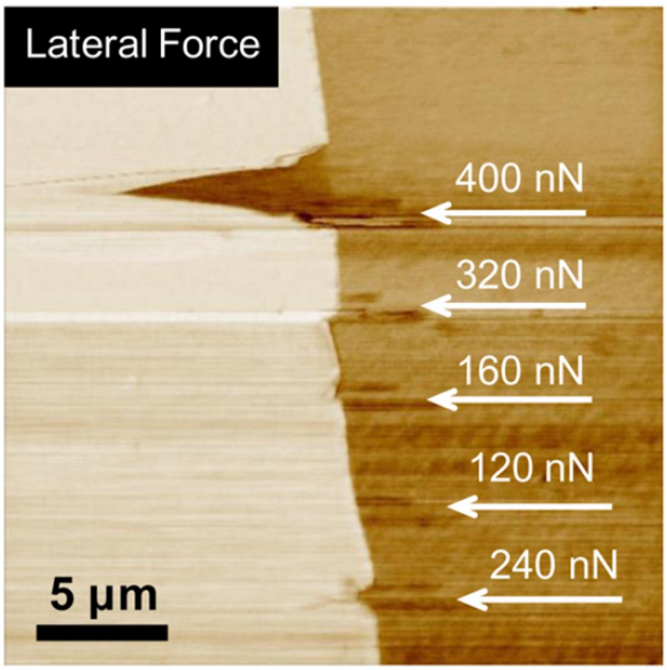

Figure 2.8 LFM image of single-layer graphene layer after scratch test at the edge of the flake. The delamination of graphene flake can be observed in the image.

Chapter 3 Preparation of specimen: graphene, CNT matrix, and graphene on CNT matrix.

3.1 Preparation of atomically thin graphene flake

Atomically thin graphene flakes were mechanically exfoliated from high-quality graphite (NGs) in order to get the desired properties. The detachment of the graphene layer from the bulk was accomplished with the help of adhesive tape. The material was then placed onto a SiO_2/Si wafer with an oxide layer with a thickness of 300 nm. It was possible to obtain an atomically thin coating of graphene on the SiO_2/Si wafer due to the adhesive force between graphene and the wafer. Aspects of the graphene flakes were studied using an optical microscope (VK-X200, Keyence). Furthermore, the surface of graphene flake was meticulously studied by AFM (MFP-3D, Asylum Research) utilizing an AC240 cantilever (Olympus).

An optical microscope and an atomic force microscope (AFM) were used to measure the thickness of a graphene flake. First, the specimen was examined with an optical microscope so that the location of the specimen could be determined, and an approximate estimate of the thickness could be made based on the contrast between the graphene flake and the SiO_2/Si wafer. Figure 3.1 provides a visual representation of an example of a graphene flake (a).

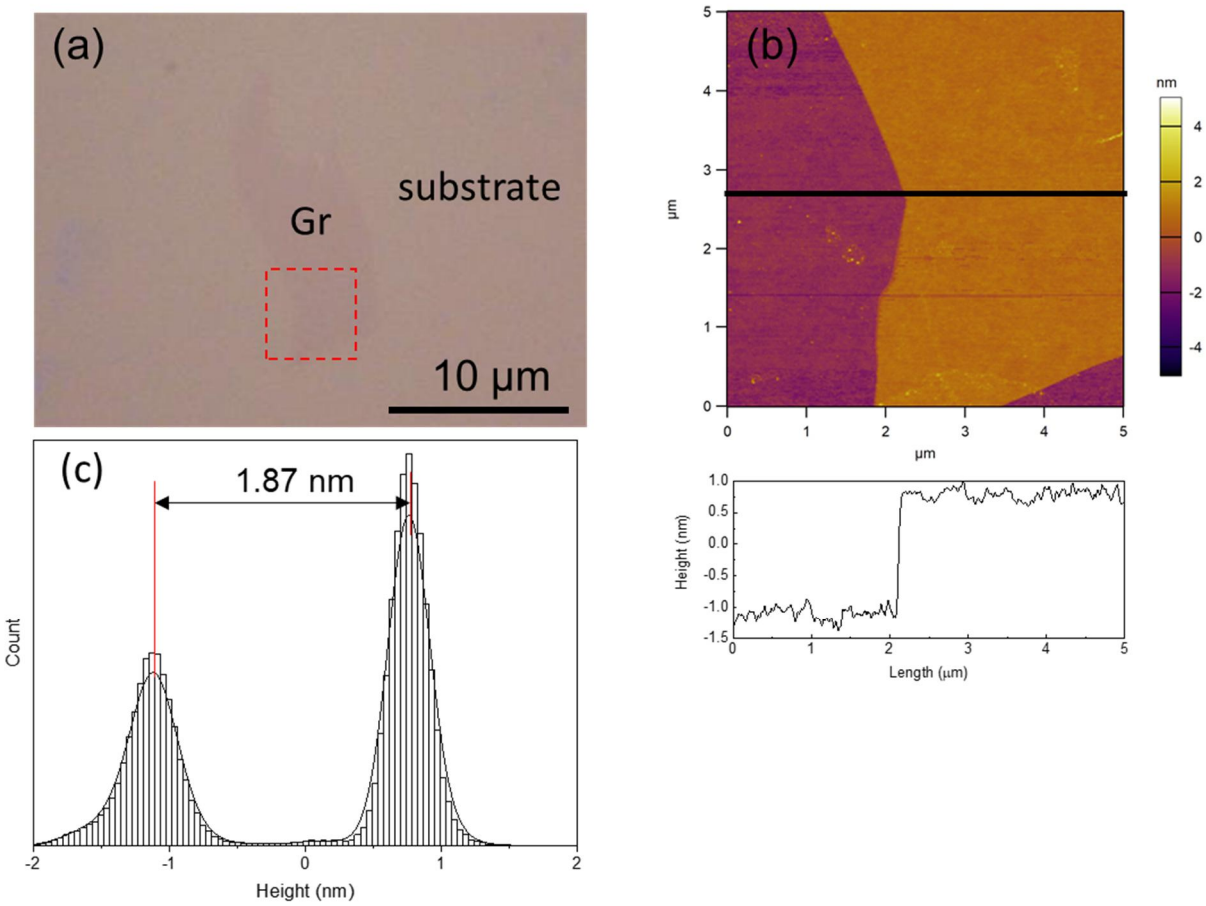

Figure 3.1 (a) Optical image, (b) AFM topographic image with corresponding cross-sectional profile and (c) histogram height from which graphene thickness was determined. Red rectangular indicate the area of graphene flake scanned with AFM AC240 probe.

After observing the graphene flake using an optical microscope, the topography of the flake was characterized with an atomic force microscope (AFM) using intermittent contact mode and an AC240 (OLYMPUS) probe. Figure 3.1 (b) displays the AFM topographic image along with the corresponding cross-sectional height profile of the graphene flake that was of interest. In order to get an accurate calculation, the height of the histogram was used to calculate the thickness of the graphene flakes. It is possible to measure the number of layers on a graphene flake by applying the flowing equation [45, 46]:

$$N = \frac{t_{measured} - 0.4}{0.335}$$

with N is number of layers, $t_{measured}$ is the thickness obtained from the histogram. Graphene flake with different thickness or number of layers was prepared and examined for investigation of friction and wear characteristics.

3.2 Preparation of CNT matrix

Figure 3.2 displays an image taken using a scanning electron microscope (SEM) of a multi-wall carbon nanotube (CNT) matrix that was coated on a SiO_2/Si wafer. It was discovered that the diameter of CNTs ranged in the region of 10 nm to 40 nm. CNT matrix was produced by employing a spinning coating deposition technique, beginning with a solution.

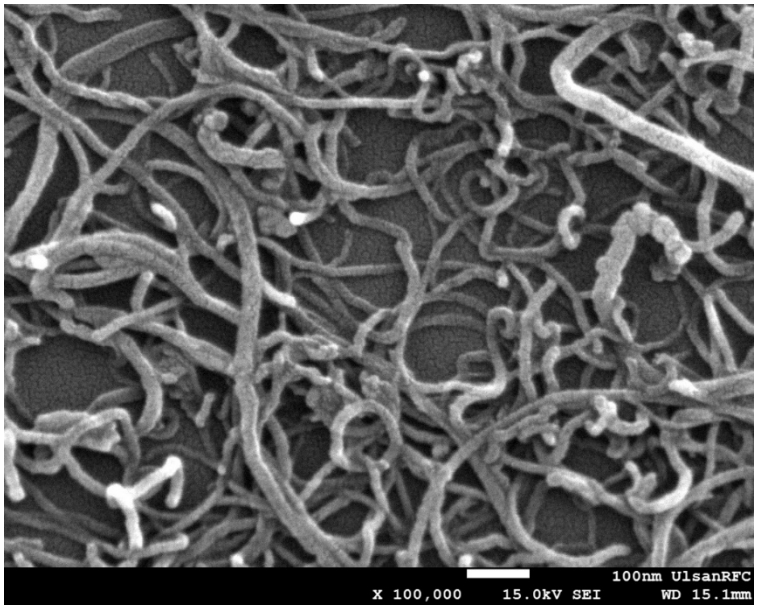

Figure 3.2 Scanning Electron Microscopy image of CNTs.

CNTs disperse in Isopropyl Alcohol (IPA) solution with concentration determined to be 0.06 % wt. was prepared for spinning coating. In order to achieve an even dispersion of the CNTs throughout the coating, the spinning speed was increased to 6000 rpm. The micropipette was used to adjust the volume of the solution to control the thickness of the CNT matrix. The volume of CNT solution was selected to 10 and 30 µL. Figure 3.3 (a) displays a topographic image of CNT grown on SiO_2/Si that was produced by AFM using the intermittent contact mode.

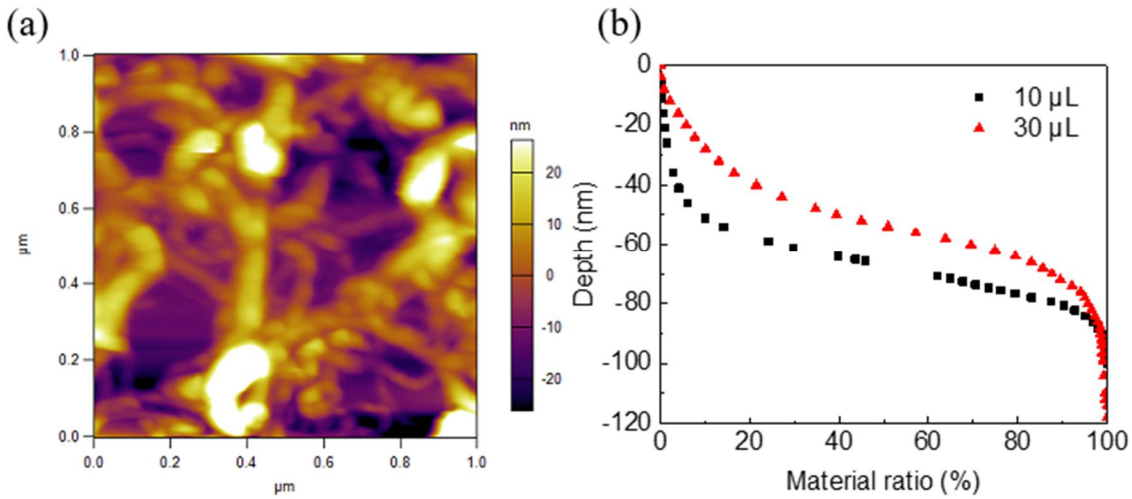

Figure 3.3 (a) Topographic image of CNT matrix and (b) material ratio of CNT matrix obtained from topographic image.

The topographic image was used to calculate the thickness of the CNT matrix in addition to the material ratio. It was found that the thickness of the CNT matrix ranged from 20 nm to 80 nm, and that the volume of the solution ranged from 10 µL and 30 µL, respectively. In addition to this, the material ratio of the CNT matrix was analyzed and plotted in Figure 3.3 (b). As was to be expected, the increase in volume of the solution results a corresponding rise in the density of the CNTs.

3.3 Preparation of 1D/2D hybrid-structure specimen

Figure 3.4 depicts the procedure for preparing a 1D/2D hybrid-structure specimen and demonstrates the steps involved. Following the determination of the thickness of the graphene flake, the SiO_2/Si wafer containing the graphene flakes of interest was coated with PMMA in preparation for the transfer procedure. During the spinning coating process, 10 μL of PMMA solution was dropped onto the SiO_2/Si wafer. The speed of the spinning coating was fixed at 3000 rpm. After spinning coating, the specimen was allowed to dry for 5 minutes in the open air. The mechanical exfoliation method was used to remove the PMMA layer from the SiO_2/Si wafer that had been created in the previous phase of the process. Peeling the PMMA layer off was made easier by applying adhesive tape to it. Because of the adhesion between the graphene flake and the PMMA layer, the graphene layer was able to separate from its substrate. It is note that for the success of separation between graphene flake and SiO_2/Si wafer, the wafer was pre-treated by immersion in piranha solution for 3 hours. The wafer was then cleaned by DI water and annealed to remove the water prior deposition of graphene. After that, a PMMA layer containing graphene was mechanically placed on top of the CNT matrix. The wafer was then subjected to a 5-minute heat treatment at 150 degrees Celsius to promote adherence of the PMMA layer to the CNT matrix layer. By immersing the PMMA layer in hot acetone (80 degrees Celsius) for three hours, the PMMA layer was completely dissolved. As a result, the graphene flakes were placed onto a CNT matrix layer to complete the process. Topographic image of graphene flake on CNT matrix was shown in Figure 3.5 (b).

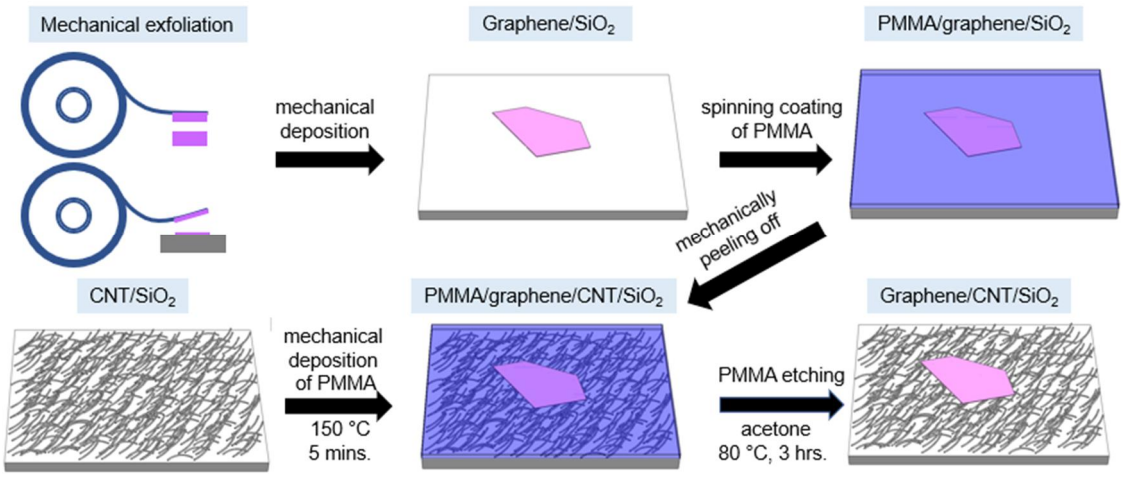

Figure 3.4 Schematic diagram of the preparation of 1D/2D hybrid-structure specimen.

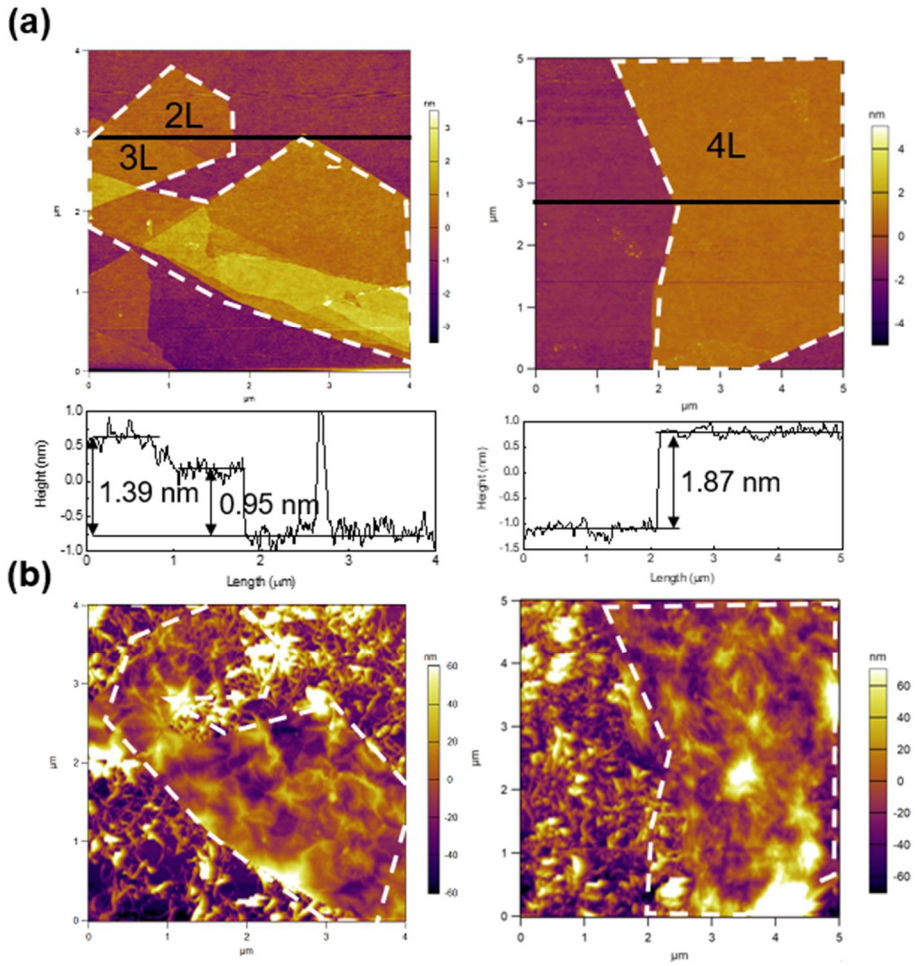

Figure 3.5 Topographic images of (a) graphene on SiO_2/Si wafer before material transfer process and (b) on top of CNT matrix after the process.

Chapter 4 Investigation of friction and wear properties of 2D and 1D/2D materials

4.1 Introduction and objectives

Researchers are always looking for ways to improve the characteristics of 2D materials in order to achieve superlubricity state. It has been suggested that one of the most essential components in the formation of superlubricity state is the lowering of shear stress at the contact zone during contact. When graphene and a hydrophobic self-assembled fluoroalkyl monolayer in water were mixed, the friction coefficient between the two materials was as low as 0.0003 when the two materials were used [47]. In addition, superlubricity state between diamond-like and graphene may be accomplished at the macroscale with the aid of nano-diamonds for the development of nano-scroll [48]. It is also feasible to tune graphene friction at the suspended area by applying in-plane tension to the flake [49, 50], in addition to the previously mentioned techniques.

The damage of 2D materials occurs when the critical contact pressure is reached, as explained in Chapter 2. The fact that this phenomenon occurs shows that with lower contact pressure, the wear resistance and wear characteristics of materials are more likely to be sustained. In this chapter, a 1D/2D hybrid-structure of graphene atop carbon nanotube is presented for tribological applications, with the first layer being a carbon nanotube. The nanotube functions as a nano spring, which helps to lower the contact pressure, which in turn helps to maintain the surface of the coating layer's coating layer. In this study, the friction characteristics of atomically thin graphene and 1D/2D hybrid-structure (graphene on carbon nanotube) were carefully investigated under a variety of conditions including normal force, graphene flake thickness, and thickness of CNT matrix were carefully

investigated. It was also taken into consideration how orientation of the nanotube affects the tribological properties of specimen. In addition, the wear properties of the specimens were studied using a constant force reciprocating scratch test for investigation of wear resistance of specimen.

4.2 Friction characteristics

4.2.1 Experiment setup

Following the production of the specimen and the characterization of the topography, friction and wear properties of the specimen were comprehensively studied utilizing AFM-based friction force microscopy measurement. Figure 4.3 (a) provides an illustration of the experimental setup schematic. Under a variety of experimental conditions, including normal force, thickness of CNT matrix, and thickness of graphene flake, the frictional properties of graphene and graphene on top of CNT matrix were investigated in this body of work.

The CNT matrix was prepared with 20 nm and 80 nm thicknesses. On a SiO2 substrate and atop a CNT matrix, graphene flakes with thicknesses ranging from 0.9 nm to 1.8 nm, corresponding to 2 layers and 4 layers, were fabricated. In addition, the orientation-dependent heterogeneous frictional properties of 1D/2D specimens were taken into account. Particularly, the frictional qualities of the specimen were studied with the AFM cantilever sliding parallel and perpendicular to the axis of the CNT.

Figure 4.1 displays topographic views of bilayer graphene on CNT matrix with varying thickness. Also, the surface roughness of the specimen was estimated based on the images. The roughness was determined using an area of 200 nm × 200 nm. The surface roughnesses were measured to be 5,5 nm and 4,8 nm with a CNT matrix thickness of 20 nm and 80 nm, respectively. The surface roughness of the specimen decreased slightly as the thickness of the CNT matrix increase.

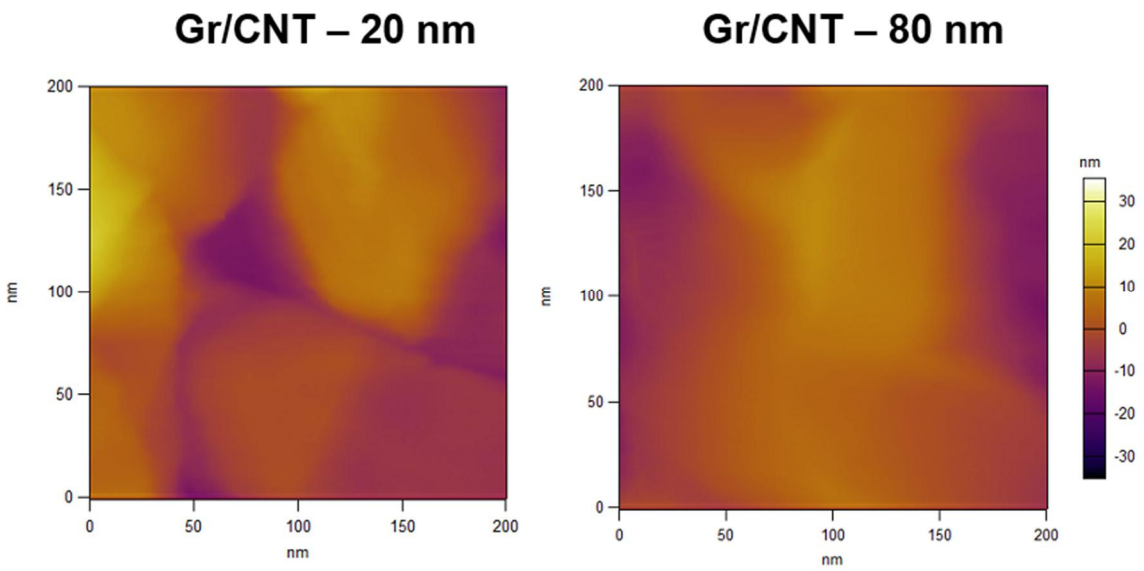

Figure 4.1 Topographic images of bi-layer graphene on CNT matrix with different thickness.

Figure 4.2 displays topographic images of graphene with different thickness on a SiO_2 substrate. The thickness of graphene flakes was also determined using topographic images, allowing the determination of the number of layers [45, 46]. The thickness of graphene flakes with two, three, and four layers was determined to be 0.94 nm, 1.35 nm, and 1.80 nm, respectively. For the study of friction, a similar thickness of graphene flake on CNT matrix was also prepared.

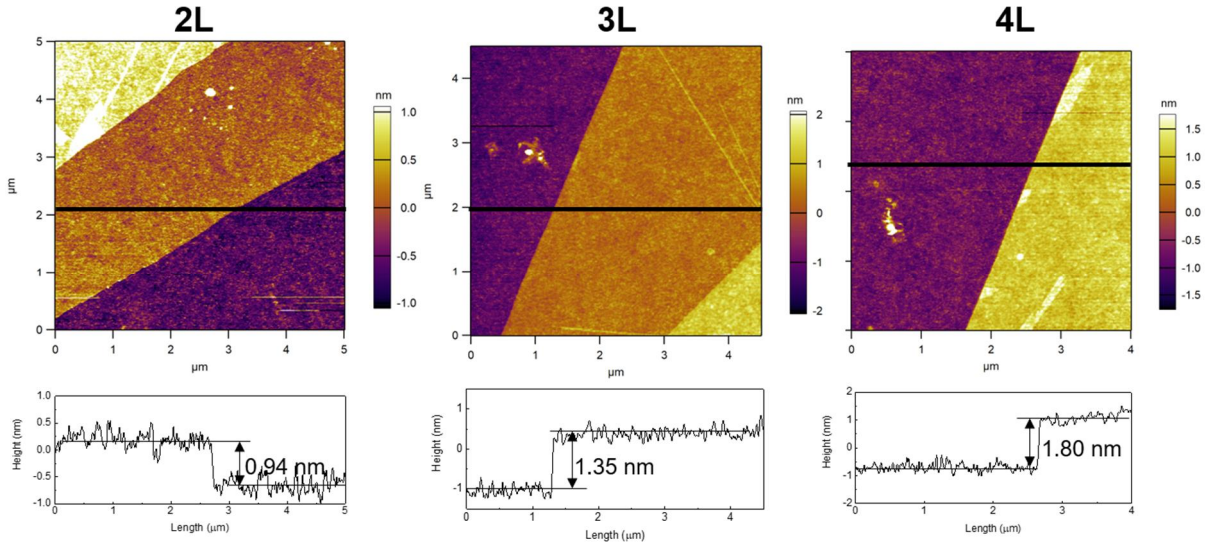

Figure 4.2 Topographic images of graphene on SiO_2 substrate with corresponding cross-sectional height profile.

For the purpose of friction characterization of the specimen, an AFM-based friction force microscope measurement was performed using a doped silicon cantilever (PPP-LFMR, Nanosensors), as can be seen in Figure 4.3. (b). For the purpose of conducting quantitative force measurements, the cantilever was calibrated in both the normal [22] and lateral directions [51, 52]. The normal spring constant of the cantilever was determined to be 0.3 N/m, and its lateral sensitivity was calculated to be 4.71 mV/nN, based on the results of the calibration. It was decided that the normal force would be in the range of 0 to 20 nN. The scan area was set to be 200 x 200 nm, and there were 128 scan lines total. The sliding speed was fixed in at a constant of 500 nm/s. Because changes in contact pressure could impact the friction characteristics of specimens, the tip wear was monitored very carefully [53]. Specifically, friction and adhesion between the tip and the graphene were evaluated both before and after the experiment.

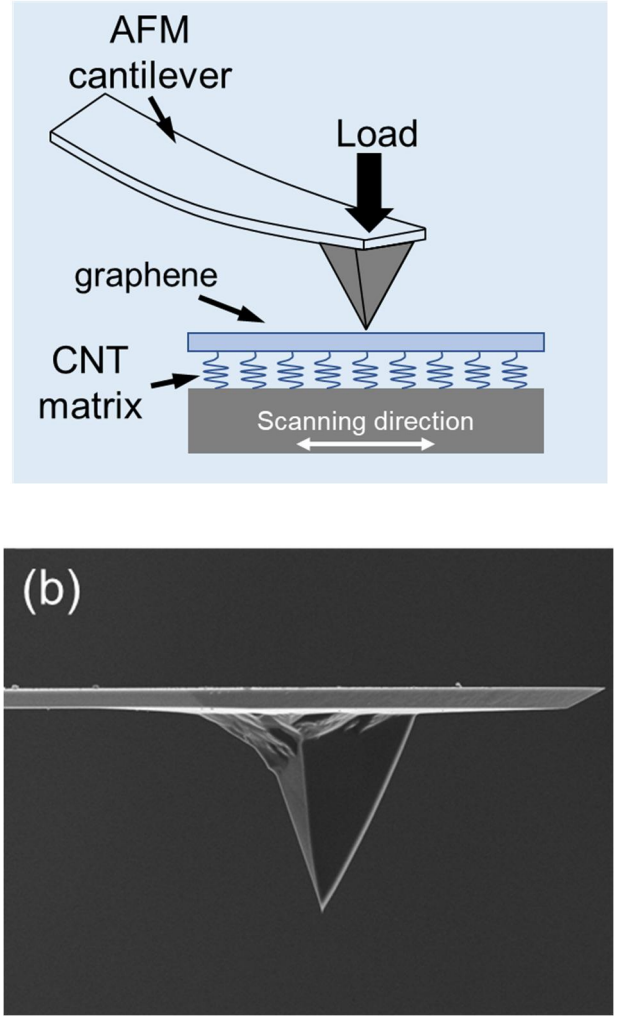

Figure 4.3 (a) Illustration of experimental setup and (b) SEM image of an AFM cantilever (PPP-LFMR, Nanosensors) used for friction force measurement.

4.2.2 Influence of thickness of CNT matrix in 1D/2D hybrid-structure

Figure 4.4 displays friction force microscope images (FFM) of bi-layer graphene on SiO_2 substrate and on CNT matrix when subjected to a normal force of 10 nN, together with the corresponding cross-sectional lateral force profile. According to the results of a cross-sectional friction force profile analysis, graphene on CNT matrix exhibits lower friction than graphene on SiO_2 substrate. Graphene on SiO_2 substrate was discovered to have a large friction force, yet the friction force profile was calmer. The friction caused by graphene on CNT matrix is decreased, but the variation is still evident. As the thickness of the CNT matrix increases, it is possible that the fluctuation of friction force that is related with the topographical effect will be minimized.

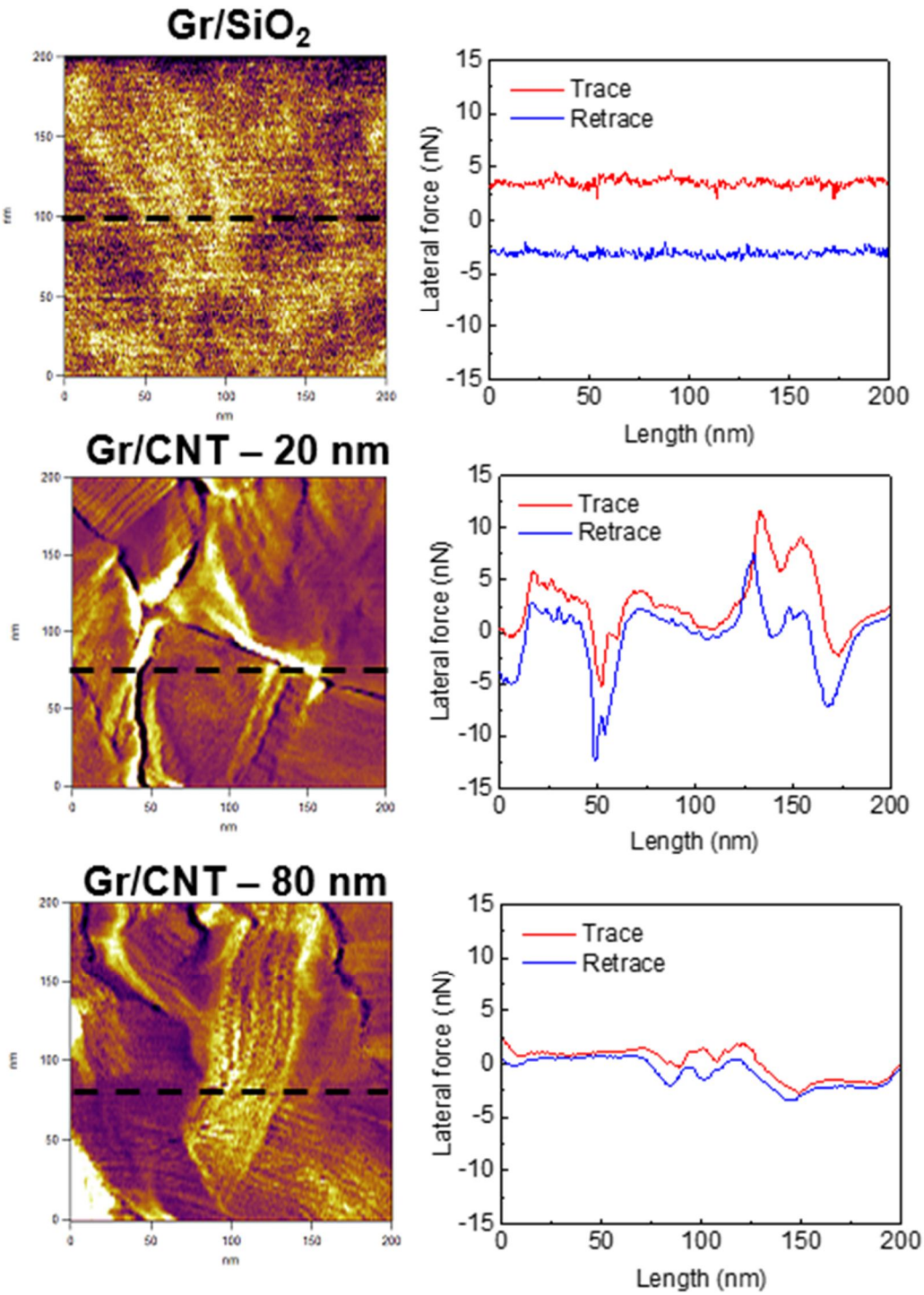

Figure 4.4 FFM images of bi-layer graphene on SiO_2 substrate and on CNT matrix with different thickness at 20 nm, and 80 nm, respectively, with corresponding cross-sectional lateral force profile under 10 nN normal force.

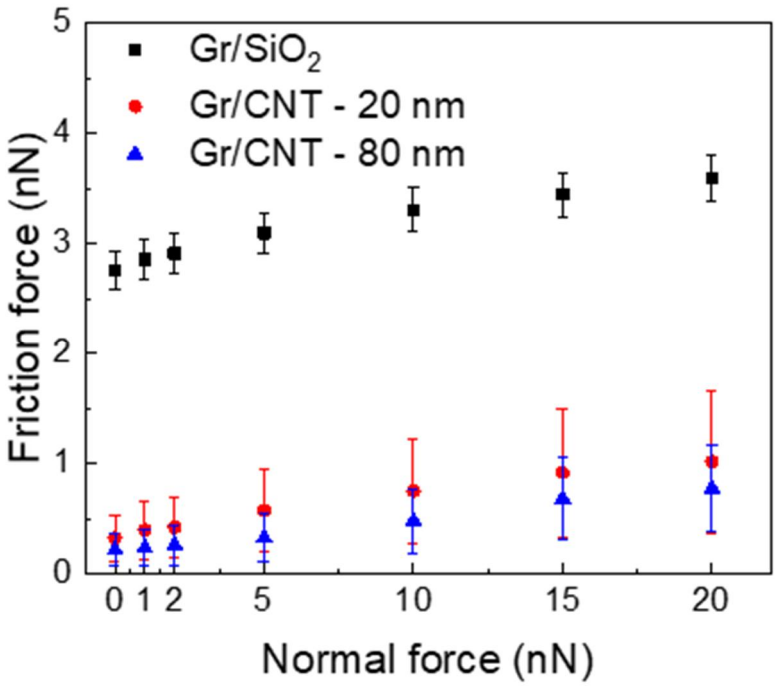

Figure 4.5 Friction force of bi-layer graphene on SiO_2 substrate and on CNT matrix with different thickness as a function of normal force.

The friction force with respect to normal force of bi-layer graphene on SiO_2 substrate and on CNT matrix with different thickness was shown in Figure 4.5. Friction force of specimen increase with increasing of normal force from 0 nN to 20 nN, as expected. In addition, friction forces of graphene on SiO_2 substrate were constantly larger than those of graphene on CNT matrix, as can be seen in the figure. In particular, with thickness of CNT matrix at 20 nm, friction force increases from 0.53 ± 0.37 nN to 1.58 ± 1.15 nN as normal force increase from 0 nN to 20 nN. With thickness of CNT matrix at 80 nm, friction force increases from 0.27 ± 0.15 nN to 1.02 ± 0.50 nN as normal force increase from 0 nN to 20 nN.

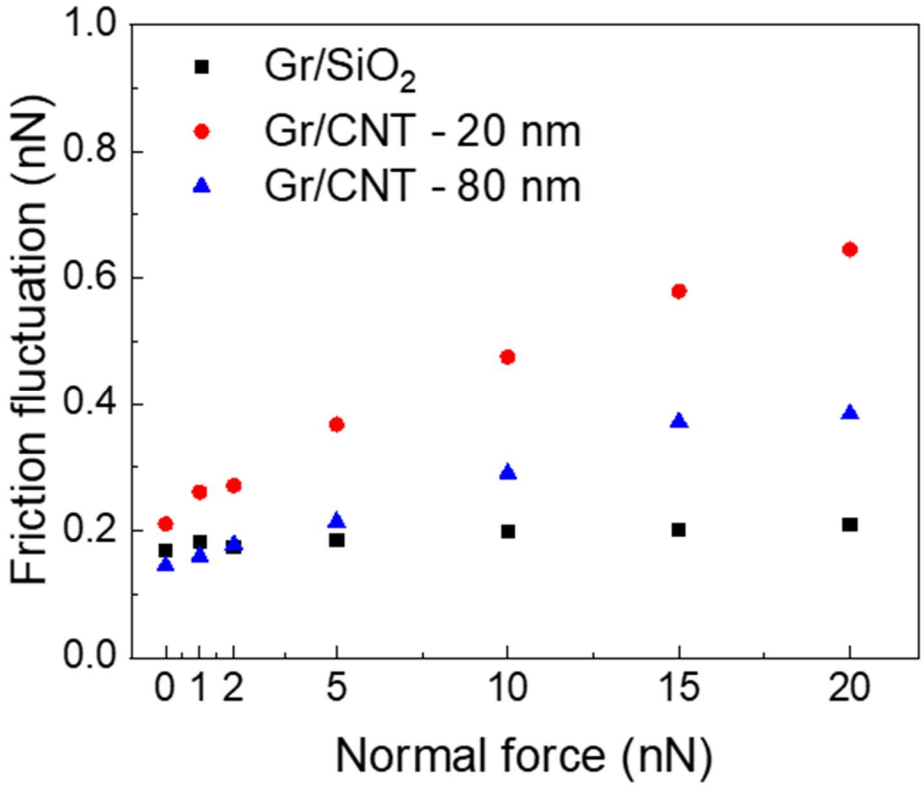

Figure 4.6 Fluctuation of friction force of bi-layer graphene on CNT matrix with different thickness as a function of normal force.

Although the thickness of the matrix did not have a significant effect on the average friction force of graphene on CNT matrix at a specific applied normal force, it did have a substantial effect on the fluctuation of friction. Figure 4.6 shows that the fluctuation of friction caused by graphene on CNT matrix of varying thickness. It was noticed that the friction force increased in a linearly in relation to the increase in the normal force. It was discovered that increasing the thickness of CNTs helps to lessen fluctuations in the force of friction, which may be partially connected with the influence that topography has on friction. It is likely that increasing the CNT matrix together with the fiber density may assist lessen the influence that topography has on friction, which will in turn lead to a reduction in fluctuation.

4.2.3 Influence of number of layers of 2D material

Friction characteristic of graphene with different thickness on SiO_2 substrate and on CNT matrix was investigate under normal force from 0 nN to 20 nN. Friction force microscope image of graphene with different thickness on SiO_2 substrate and on CNT matrix under 10 nN was shown in Figure 4.7.

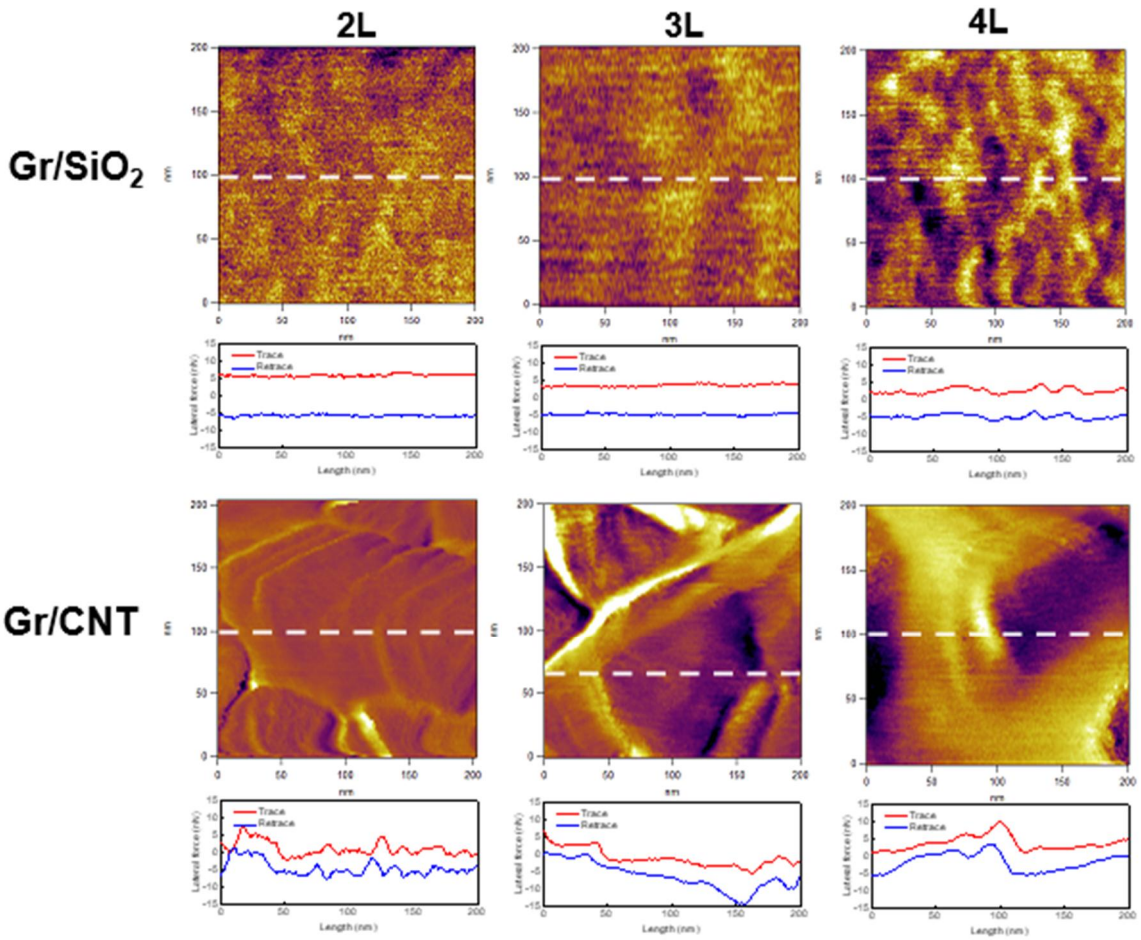

Figure 4.7 FFM images of graphene with different thickness on SiO_2 substrate and on CNT matrix under 10 nN normal force.

In general, friction force profile was found to be calm with graphene on SiO_2 substrate. Although has large fluctuation, friction of graphene on CNT matrix was found to be smaller which agree with previous data. Decrease of friction with increasing of number of layer or thickness of graphene was observed with both specimens. The decrease of friction can be clearly observed in Figure 4.8.

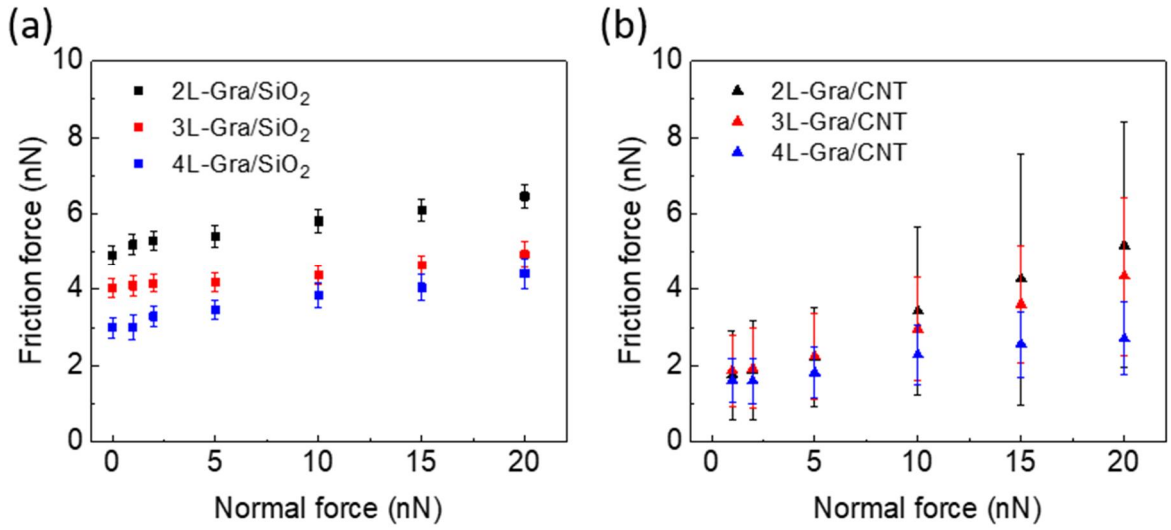

Figure 4.8 Friction force as a function of normal force of graphene with different thickness on SiO_2 substrate and on CNT matrix.

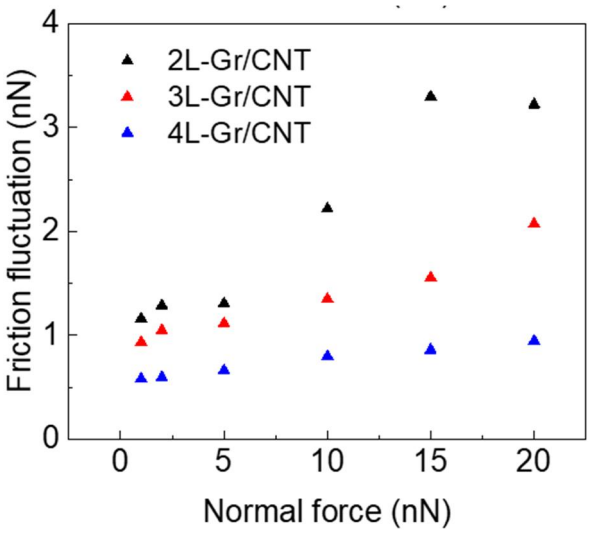

Figure 4.9 Fluctuation of friction of graphene with different thickness on CNT matrix.

In addition, it was found that increase of graphene thickness also help to reduce in fluctuation of friction. This behavior could relate interaction between AFM tip and graphene flake. In particular, bending stiffness of graphene flake increases with increasing of thickness could help to reduce puckering effect which resulted in decrease of friction [54]. In addition, increase of bending stiffness could also help to reduce the formation of wrinkle, so that effect of topography on friction could be minimized. This behavior could respond for the decrease of fluctuation of friction force of graphene on CNT with calmer friction force profile of thicker graphene flake on CNT, as can be seen in Figure 4.7, Figure 4.8, and Figure 4.9.

4.2.4 Heterogeneous friction properties of graphene on CNT matrix

To further investigate influence of orientation on frictional properties of 1D/2D hybrid structure, the FFM measurement was conducted with 2 different scanning directions as same location. The FFM measurement was carried out with two distinct scanning directions at the same site so that further investigation could be done into the influence of orientation on the frictional properties of a 1D/2D hybrid construction. The longitudinal direction denotes a parallel relationship between the direction of scanning and the axis of the CNT. Similarly, the transverse direction in which the scanning direction and the axis of CNT are perpendicular to one another. The FFM images that were acquired in the longitudinal and transverse directions of the CNT are displayed in Figure 4.10, together with the accompanying histogram of the local friction force.

The FFM images clearly show friction in longitudinal direction is smaller than that in transverse direction. In addition, large contrast in FFM image of transverse direction implies large fluctuation of friction force. This behavior could be related to topography-

induced friction effect where friction force was different when climb and go down the edge cause by CNT, as discussed above. Histogram at local area in longitudinal and transverse scanning direction was plotted in Figure 4.10(c). The histogram clearly shows confirm smaller friction in longitudinal direction. Friction force of bi-layer graphene on SiO_2 substrate was used as reference to clarify effect of CNT matrix on frictional properties of graphene. Figure 4.10(c) shows friction force was reduced in both scanning directions compared with that of graphene on SiO_2 substrate. Furthermore, friction of graphene at suspended area was also found to be reduced, as can be seen in the figure.

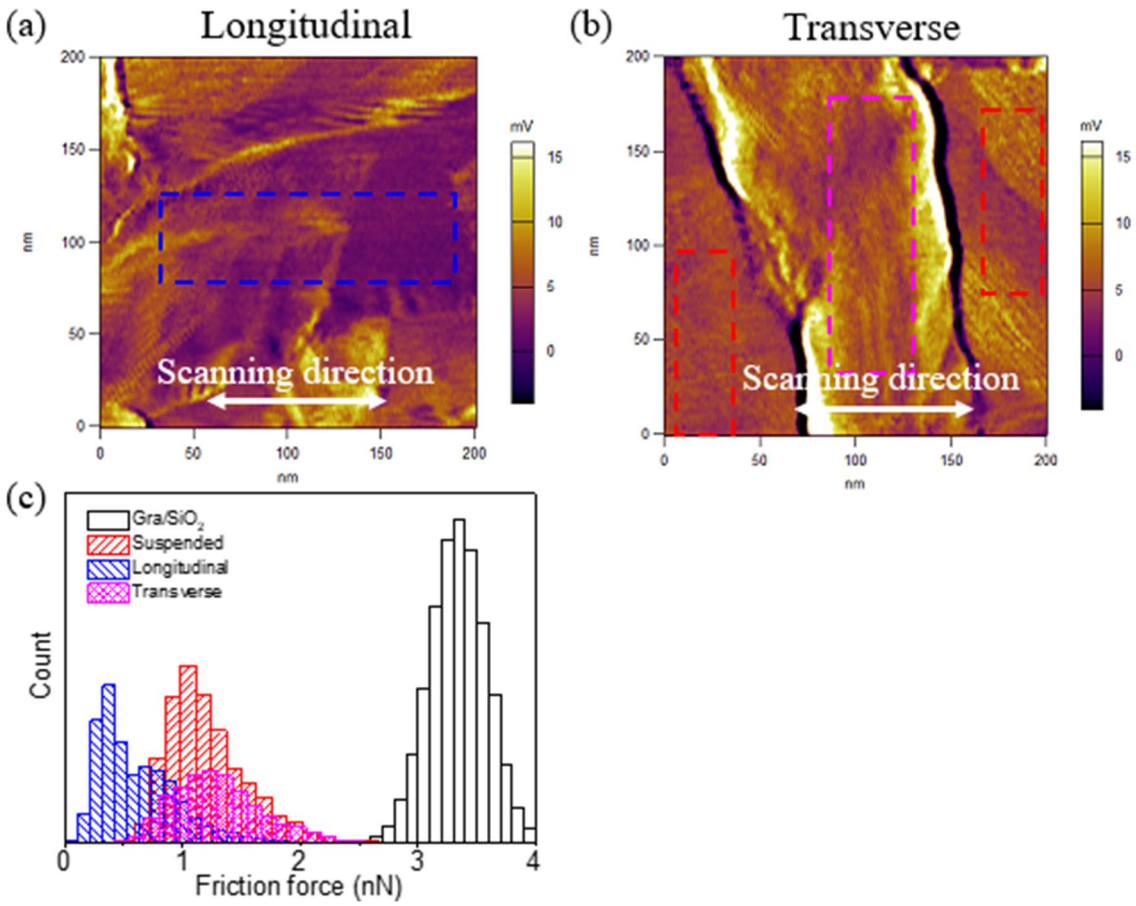

Figure 4.10 FFM images obtained in (a) longitudinal and (b) transverse scanning direction, (c) histogram of friction force at local area of bi-layer graphene on a CNT.

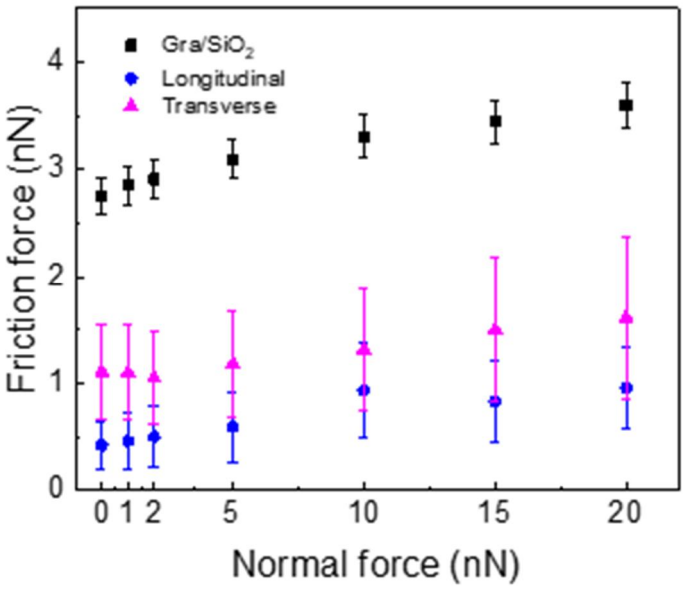

Figure 4.11 Friction force of bi-layer graphene on SiO_2 substrate and on CNT as a function of normal force in longitudinal and transverse scanning directions.

The influence of orientation of CNT was further investigated under various normal force. Friction force of bi-layer graphene on SiO_2 and on CNT in longitudinal and transverse scanning directions with normal force ranging from 0 nN to 20 nN was shown in Figure 4.11. Friction force on specimens increase with increasing of normal force, as expected. The smaller of friction force of graphene on CNT in longitudinal was smaller than that in transverse scanning direction, which agree with data in Figure 4.10. In addition, friction forces of bi-layer graphene on CNT in both scanning directions was found to be constantly smaller than those of graphene on SiO_2 substrate with the range of normal force from 0 nN to 20 nN. In particular, friction force of bi-layer graphene on CNT in longitudinal, transverse scanning directions, and on SiO_2 substrate increase from 0.42 ± 0.22 nN to 0.96 ± 0.39 nN, from 1.11 ± 0.44 nN to 1.62 ± 0.76 nN, and from 2.76 ± 0.17 nN to 3.60 ± 0.21 nN, respectively, with normal force increase from 0 nN to 20 nN.

Large fluctuation of friction which associated with the topography-induce friction effect can also be seen in Figure 4.11. The fluctuation of friction in transverse scanning direction was found to be larger than that in longitudinal scanning direction. In particular, standard deviation of friction force is from 0.22 nN to 0.39 nN, and from 0.44 nN to 0.76 nN, respectively. For graphene on SiO_2 substrate, the standard deviation of friction force was found to be about 0.19 nN with normal force ranging from 0 nN to 20 nN. This result suggests that CNT matrix could be beneficial for friction reduction of atomically thin graphene. In addition, the friction reduction could be more effective in longitudinal direction than transverse direction with smaller and less fluctuate of friction force.

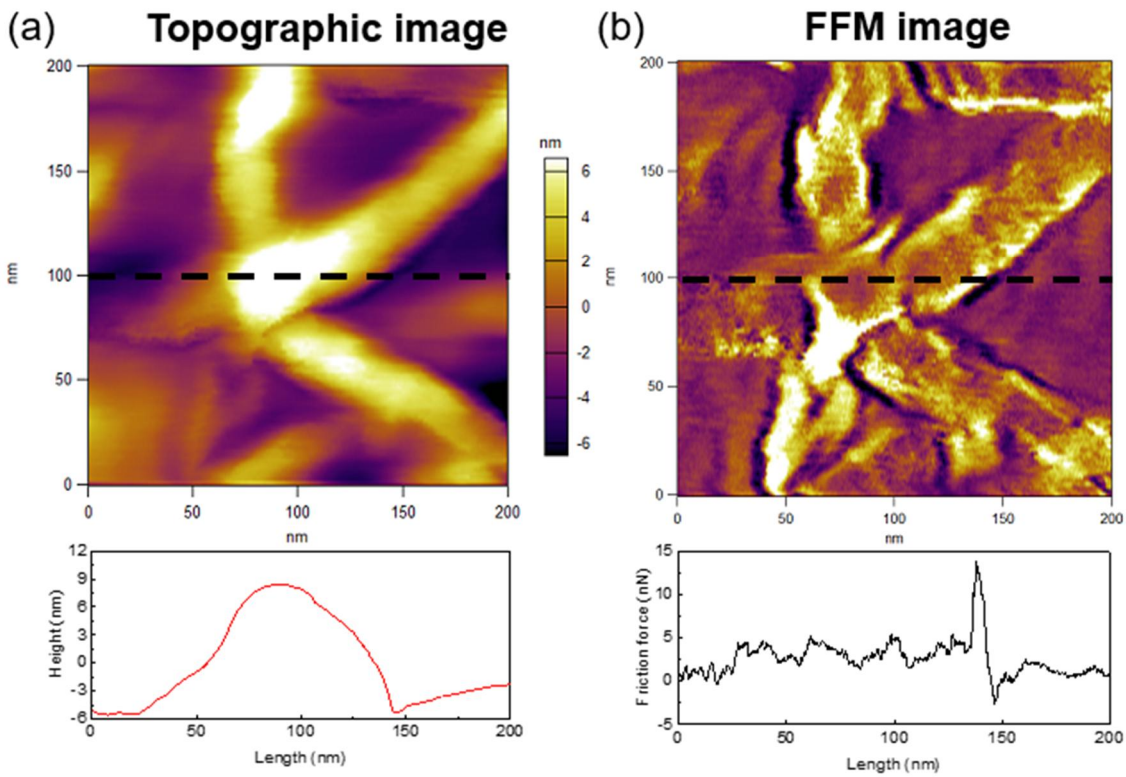

Figure 4.12 (a) Topographic and FFM images of graphene on CNT matrix at intersection of two CNTs.

To further understand heterogeneous friction properties of graphene on CNT matrix, FFM measurement of graphene on intersection of two CNTs was conducted. Friction force was found to be increase at the intersection area, regardless scanning direction was remained on same CNT, as can be seen in Figure 4.12. This behavior implies heterogeneous of graphene on CNT matrix was not only affected by CNT at interface, but also CNTs below the structure.

4.2.5 Topography-induce friction of graphene on CNT matrix

Figure 4.13 (a) shows a topographic image of graphene flake on a CNT. The shape of cross-sectional profile in trace and retrace direction was found to be similar to each other, as shown in Figure 4.13 (b). The tip moves from left to right in trace direction and from right to left in retrace direction. In addition, the cross-sectional profile indicates large variation in height of specimen topography. The derivative of cross-sectional height profile was also calculated and plotted in Figure 4.13 (c). Friction force microscopy (FFM) image at the same location of specimen was also collected and plotted in Figure 4.13 (d). Variation of friction force was clearly indicated in the figure. The friction loop from FFM image was shown in Figure 4.13 (e). It was found that the shape of friction loop was similar with that of derivative obtain from cross-sectional height profile. This behavior can be explained by ratchet mechanism in which difference in friction between the tip encounter incline and decline slope. In particular, the variation of friction force is associated with normal force and slope of topography as $F_F \sim tan\delta \times F_N$ where $tan\delta$. It may require more friction for the when the tip ascending the leading edge with positive slope. In contrast, when encounter

trailing edge, the slope becomes negative lead to decrease of friction. In addition, the fluctuation of friction force could be contributed by “collision” in which friction is higher when the tip climbing up the asperity comparing with going down [20].

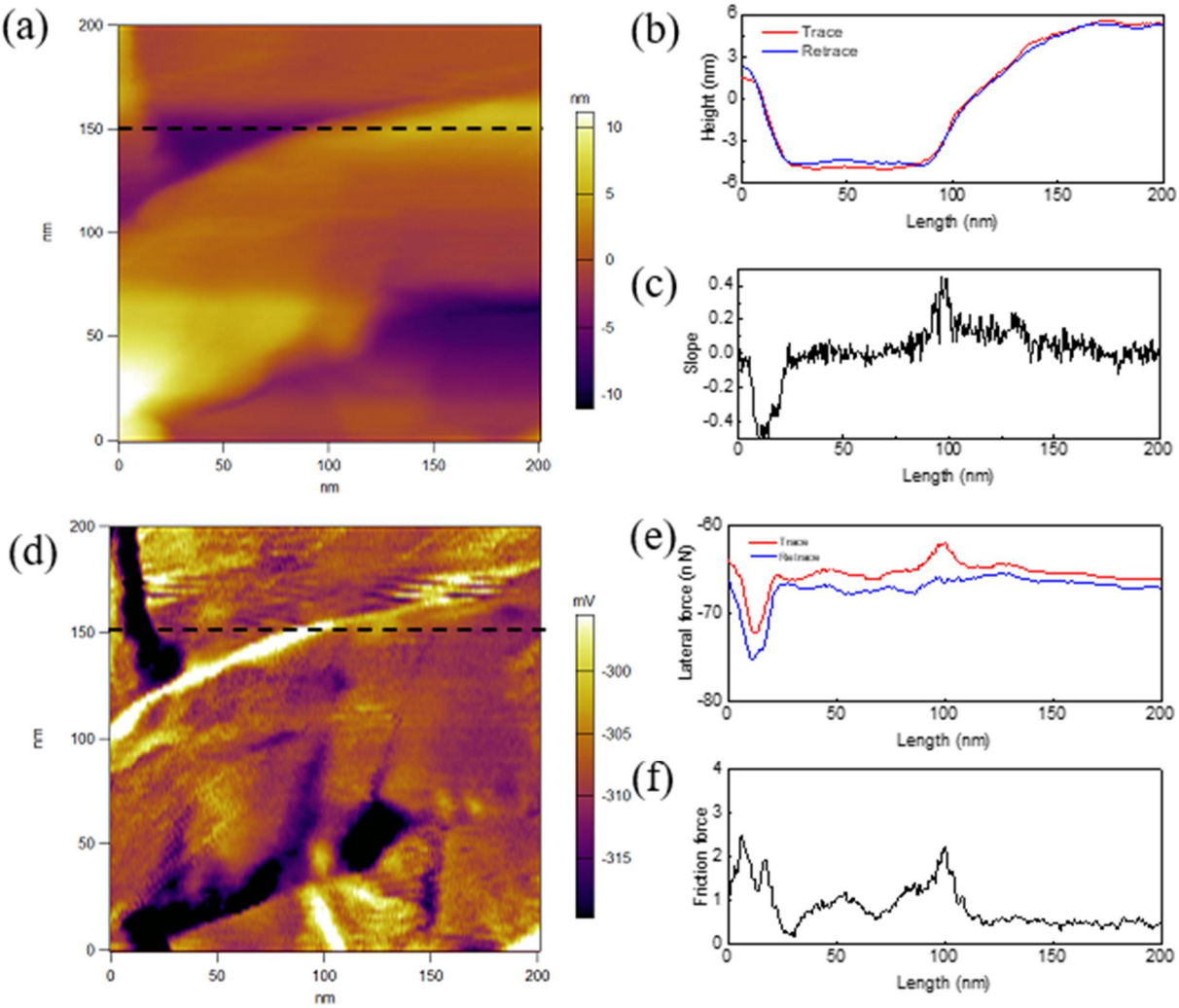

Figure 4.13 (a)Topographic image of graphene flake on a CNT with (b) corresponding cross-sectional height profile and (c) derivative of cross-sectional height profile. (d) Friction force microscope image with (e) cross-sectional later force profile and (f) friction force profile. Friction force profile was calculated by half of lateral profile in trace and retrace direction.

4.2.6 Discussion

Frictional properties of graphene on SiO_2 substrate and on CNT matrix was systematically investigated under various conditions, such as CNT matrix thickness, graphene thickness, and normal force. The result shows that friction of graphene on CNT matrix was consistently smaller than that of graphene on SiO_2 substrate. The decrease in friction of graphene on CNT matrix could be contributed by various factor, such as in-plane strain of graphene flake due to transfer process or during contact with AFM tip, or interaction between graphene and CNTs. For instant, the partial support of CNT matrix could help to generate in-plane strain of graphene flake during contact with AFM due to deformation, as illustrated in Figure 4.14. Decrease of friction with increase of in-plane strain of graphene was reported in [50].

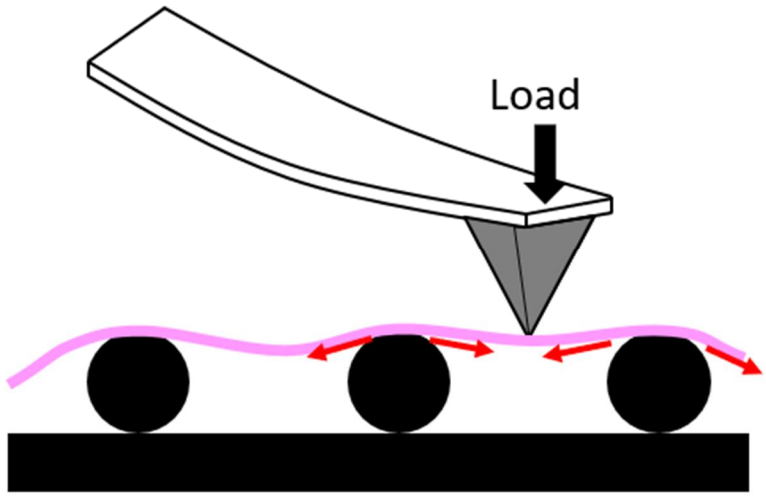

Figure 4.14 Illustration of contact between AFM tip and graphene on CNT matrix.

In addition, absent of friction dissipation of CNT could be contributed to the low and heterogeneous friction of specimen. This behavior could be contributed by heterogeneous frictional properties of CNTs. Marcel Lucas, et al. suggest that smaller friction in

longitudinal scanning direction is due to absent of frictional dissipation while soft rolling of the tube occurs in transverse scanning direction [55]. Decrease in friction of suspended graphene which was also observed in [49] could contributed to the overall of low friction of graphene on CNT matrix compare to that of graphene on SiO_2 substrate.

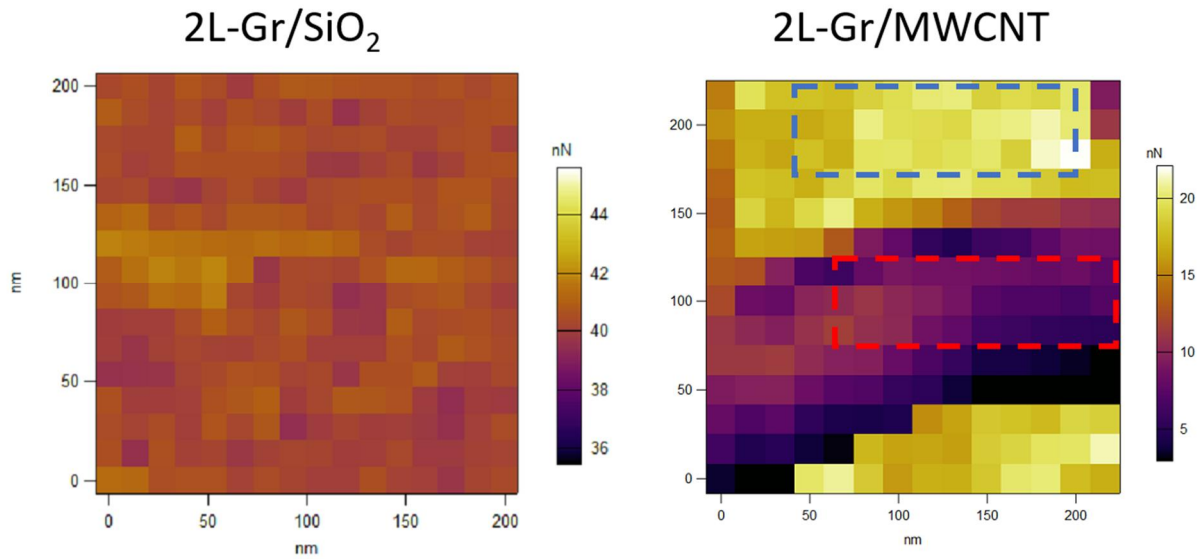

Figure 4.15 Friction force map of bi-layer graphene on SiO_2 substrate and on CNT matrix. Red and blue rectangular indicate areas of graphene CNT and suspended graphene, respectively.

Adhesion properties of specimen also contribute to friction characteristic [56]. Friction force map of bi-layer graphene on CNT matrix was shown in Figure 4.15. Large adhesion with no significant variation with respect to location was found for graphene on SiO_2 substrate. Adhesion force of bi-layer graphene on CNT matrix was found to be smaller. In addition, heterogeneous adhesion property was found for bi-layer graphene on CNT matrix, as can be seen in Figure 4.15. Lower adhesion was found for graphene on CNTs compared to that of suspended graphene. Adhesion of graphene on SiO_2 substrate and on CNT matrix with respect to location obtained from friction force map was shown in Figure 4.16. Adhesion force between AFM tip and graphene on SiO_2 substrate was found to be 40 ± 0.4

nN. Adhesion force between AFM tip and graphene on CNT matrix at on CNTs and suspended area were found to be 7.3 ± 1.6 nN and 18.7 ± 1.5 nN, respectively.

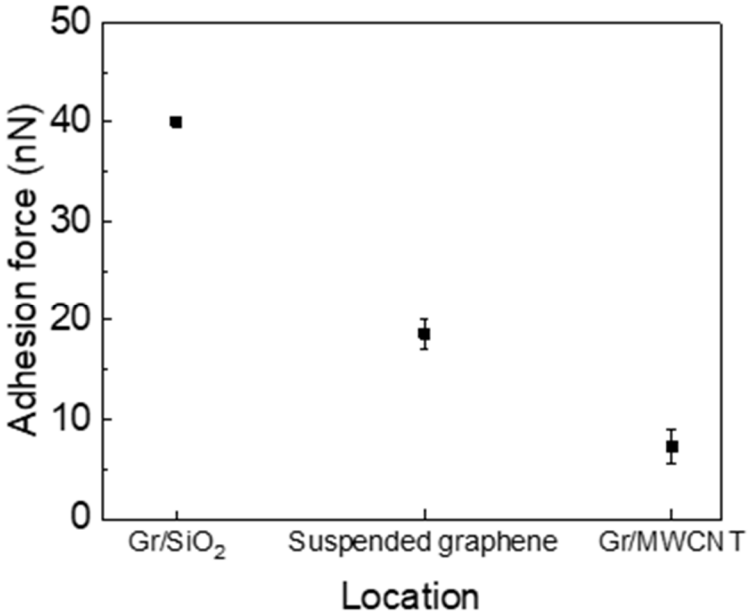

Figure 4.16 Adhesion force of bi-layer graphene on SiO_2 substrate and on CNT matrix with respect to location obtained from friction force map.

It was found that adhesion of graphene on CNT matrix increases with increasing of graphene thickness. However, decrease of adhesion with increasing of graphene thickness was found with graphene on SiO_2 substrate. In particular, for graphene on CNT matrix, adhesion increases from 4.6 ± 1.7 μN to 13.2 ± 3.3 μN with increasing number of layers of graphene thickness from 2 layers to 4 layers. For graphene on SiO_2 substrate, adhesion decreases from 35.4 ± 0.3 μN to 33.5 ± 0.4 μN with increasing number of layers of graphene thickness from 2 layers to 4 layers. This behavior implies contribution of CNT matrix on reduction of adhesion.

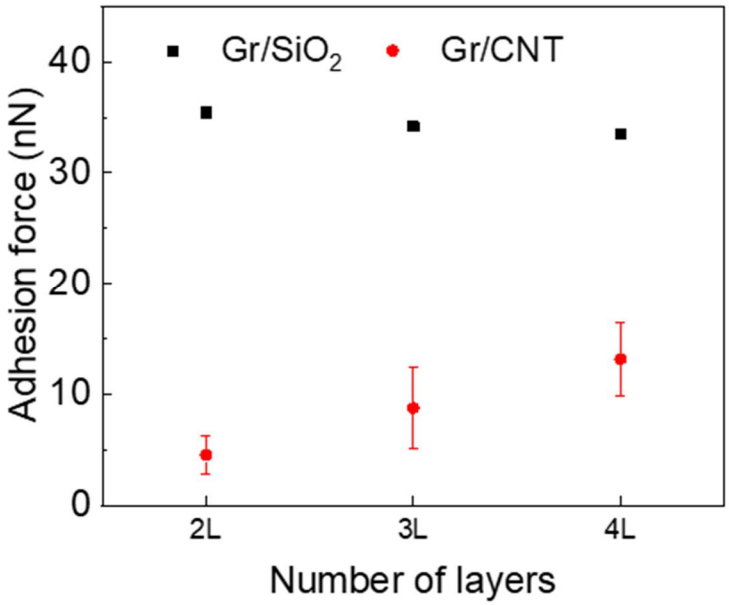

Figure 4.17 Adhesion force of graphene flake with different thickness on SiO_2 substrate and on CNT matrix

Low adhesion of graphene on CNT could be contributed by low adhesion properties of CNT which associated with low surface energy. In addition, lower adhesion with graphene on CNT compared to suspended graphene confirm low adhesion properties of the fiber. Lower adhesion of suspended graphene compared to supported graphene was also observed in [50]. Low adhesion of graphene on CNT matrix could be partially respond for the low friction of specimen. In addition, low adhesion properties may cause relative sliding between graphene and CNT or between CNT and its substrate (SiO_2 substrate) during contact with AFM tip. Relative sliding could change contact condition from between AFM tip and graphene flake to contact between AFM flake and CNT or contact between CNT and SiO_2 substrate led to decrease of friction. Similar behavior of graphene was also observed in [49, 57].

Overall, graphene on CNT possesses lower friction property compared to that of graphene on SiO_2 substrate. This behavior could relate to in-plane strain of graphene due

to compliance of graphene flake on CNT matrix. Contact between tip and graphene could also enhance to the in-plane strain of graphene flake that contributed to the decrease of friction. Due to partially support of CNT for graphene flake, the reduction of friction of suspended graphene was observed with agree with those in literature. In addition, small adhesion of graphene on CNT matrix could partially contributed to the low friction of specimen.

4.3 Wear characteristics

4.3.1 Experimental setup

For investigation of wear resistance, diamond cantilever was used in reciprocating scratch test. The diamond cantilever was carefully observed with SEM for determination of radius at the tip. The SEM of diamond tip was used in reciprocating scratch test was shown in Figure 4.18. The diamond cantilever was used with tip radius was determined to be 50 nm.

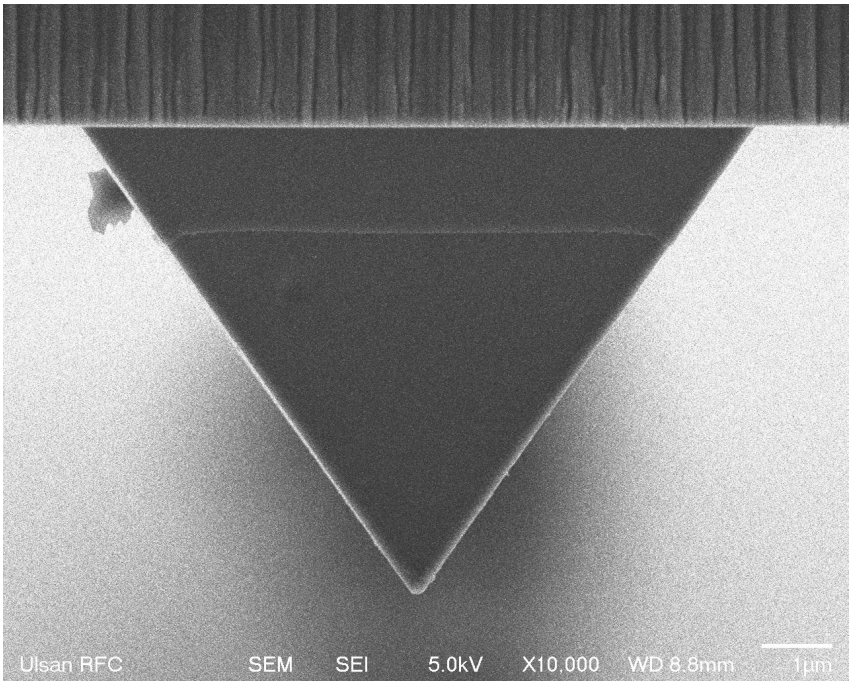

Figure 4.18 SEM image of AFM diamond tip used in reciprocating scratch test.

Constant normal force was set to be 2 μN during reciprocating scratch test. From mechanical properties of bulk diamond [58] and bi-layer graphene [59], the mean contact pressure was determined to be 21.4 GPa for bi-layer graphene on SiO_2 substrate, based on Hertzian contact theory. For graphene flake on CNT matrix, the contact pressure was expected to be smaller. The stroke of reciprocating scratch test was set to be 200 nm. The sliding speed was set at 500 nm/s. The cantilever was reciprocated with number of cycles up to 128 cycles. During reciprocating scratch test, friction force between the tip and specimen was monitored for observation of failure. Topography of specimen before and after experiment was observed after reciprocating scratch test for observation of failure. In addition, FFM measurement at tested area after reciprocating scratch test was also conducted to observe any change in friction properties of specimen. FFM image of specimen at test area using PPP-LFMR (Nanosensors) cantilever under 10 nN normal force. All experiments were conducted in ambient conditions (25 °C, 30% RH).

4.3.2 Friction behavior during and after reciprocating scratch test

Friction loop of AFM tip sliding against bi-layer graphene on SiO_2 substrate and on CNT matrix in reciprocating scratch test was shown in Figure 4.19. As can be seen in Figure 4.19, friction loop of bi-layer graphene was observed with typical shape. However, increase of friction with increasing of number of cycles was observed. In other hand, unique shape of friction loop of bi-layer graphene on CNT matrix which associated with topography effect on friction was observed. Similar shape and amplitude during reciprocating scratch test was observed with bi-layer graphene on CNT matrix specimen.

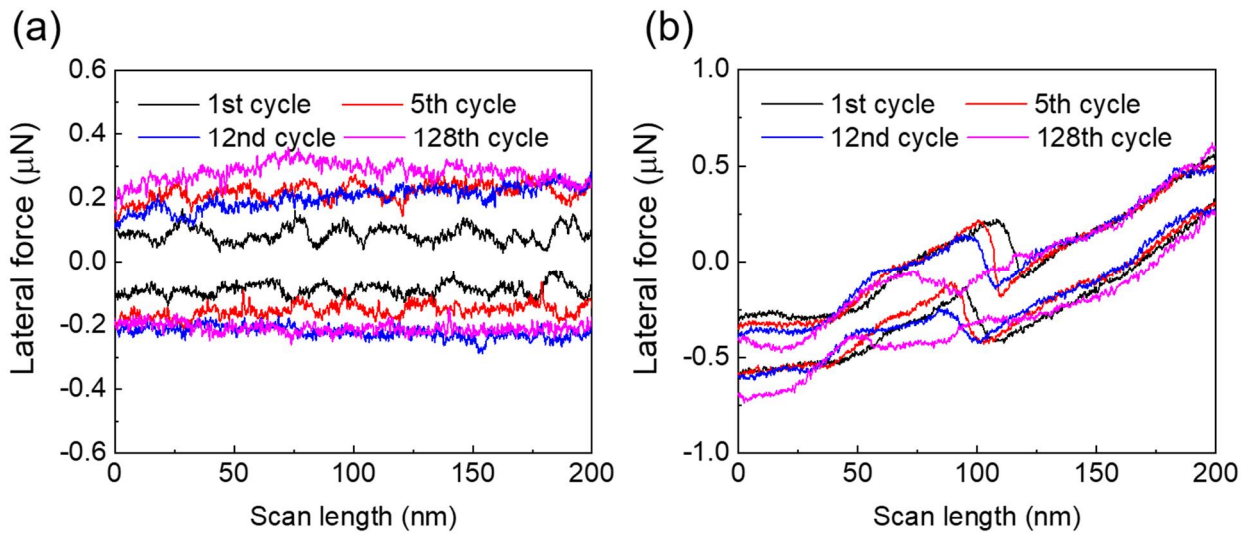

Figure 4.19 Friction loop of bi-layer graphene on (a) SiO_2 substrate and (b) on CNT matrix under 2 μN.

From friction loop, friction force as a function of number of cycles was obtained and shown in Figure 4.20. Low friction was observed at the initial stage of the test of graphene on SiO_2 substrate specimen. However, friction of graphene on SiO_2 specimen increase with increasing of number of cycles. In particular, it was found that friction of graphene on SiO_2 substrate specimen continuously increases and maintain as high as 1.27 μN after 12nd cycle

to the end of the test. The increase of friction indicates damage or failure of the coating film. For graphene on CNT matrix specimen, friction was high at initial stage. However, friction force was found to rapidly decrease with increasing of number of cycles and maintain at as low as 0.22 μN to the end of the test. High friction at the initial stage could be due to the presence of wrinkle or contaminant on the surface of specimen due to transfer process. The decrease and maintain of friction as low suggest that the coating film was intact after experiment.

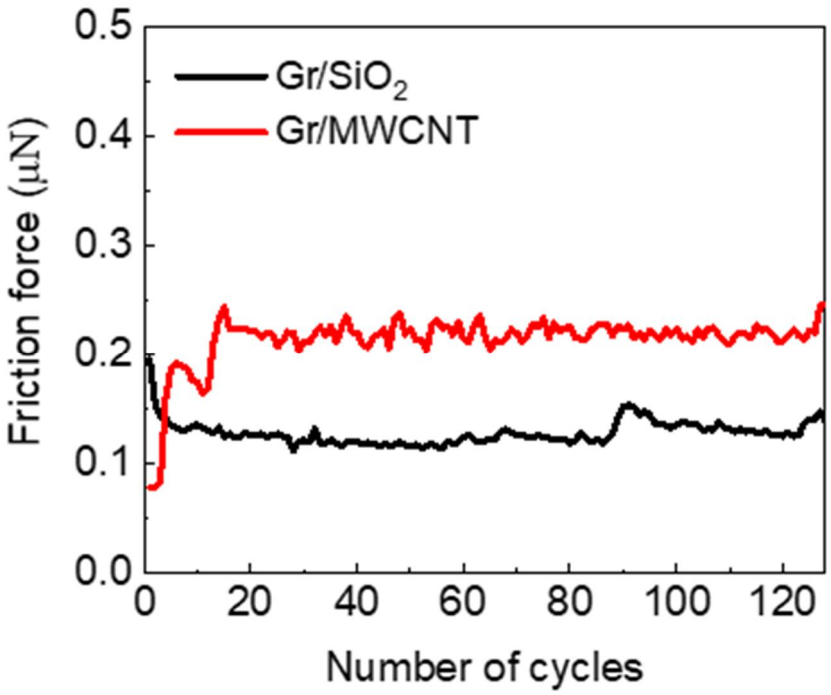

Figure 4.20 Friction force as a function of number of cycles in reciprocating scratch test of bi-layer graphene on SiO_2 substrate and on CNT matrix.

To further investigate the topography and tribological characteristics of specimen, topographic image and FFM image of specimen was obtained after reciprocating scratch test. Topographic image of bi-layer graphene after reciprocating scratch test was shown in Figure 4.21. Formation of wear track was observed in the topographic image at the scratch

test of specimen. The formation of wear track was likely due to the formation of SiO_2 substrate which typically observed after scratch test [11, 31]. The depth of wear track was found to be about 0.8 nm.

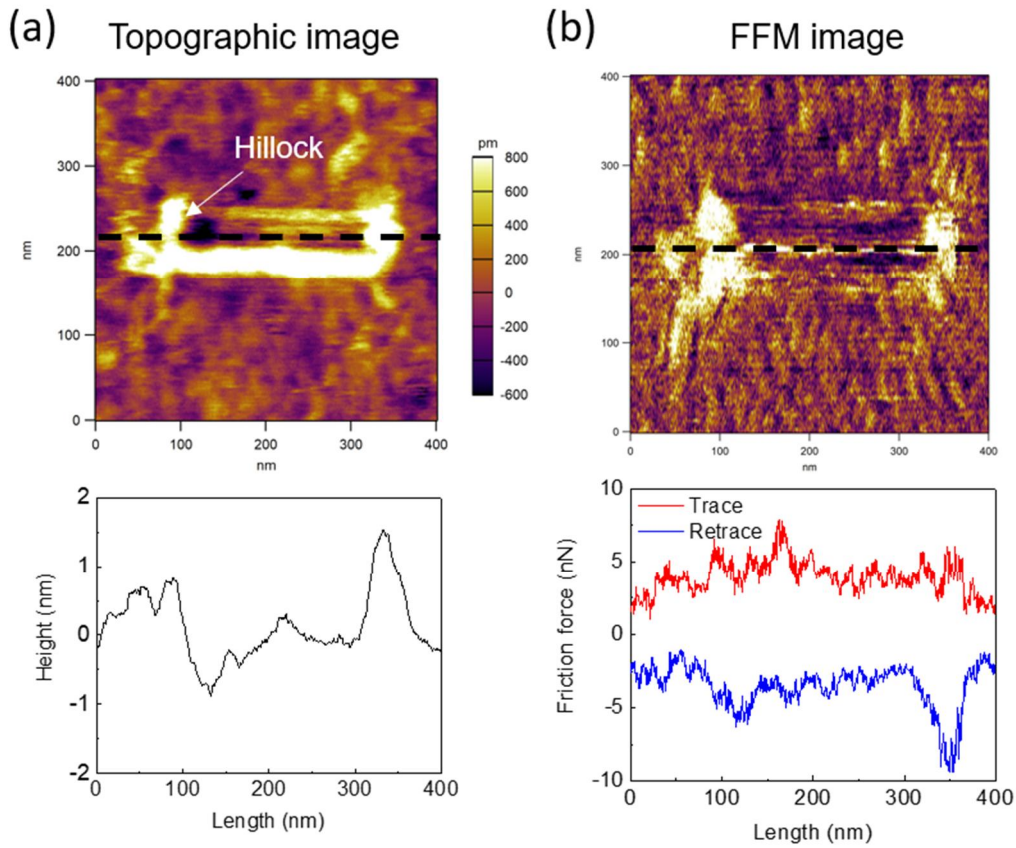

Figure 4.21 (a) Topographic and (b) FFM image of bi-layer graphene on SiO_2 substrate after 128-cycle of AFM-based reciprocating scratch test. The corresponding cross-section profiles was obtained from the images as location indicated with black-dash line.

In addition, accumulation of material along scratch test and at two-end were also observed, as can be seen in Figure 4.21 (a). Furthermore, FFM image indicates that there is difference inside and outside the scratch test area of specimen, as can be seen in Figure 4.21 (b). In addition, increase of friction was also found at hillock area. The increase of friction at scratch test area can be clearly seen in cross-sectional friction force profiles. In

particular, friction force at outside and inside wear track was determined to be 2.63 ± 0.52, and 4.80 ± 1.63 nN under 10 nN normal force in FFM measurement. This behavior suggests the change in frictional properties of specimen due to defects formation or surface damage.

Topographic and FFM images of bi-layer graphene on CNT matrix after reciprocating scratch test were also obtained. Sign of wear track formation with large deformation was also observed in topographic image, as can be seen in Figure 4.22 (a). However, the deformation after reciprocating scratch test was likely due the compliance of coating film. FFM image with corresponding friction force profile of specimen after reciprocating scratch test was shown in Figure 4.22 (b). Spikes in friction force implies there was formation of defects on surface of specimen. Spike in FFM image due to defect was typically observed with other 2D material [11, 60]. However, friction force was not significantly different between inside and outside of wear track. In particular, friction outside and inside wear track was found to be 0.45 ± 0.19 nN and 1.79 ± 1.39 nN, respectively, under 10 nN normal force. In contrast with topographic and FFM images of bi-layer graphene on SiO_2 substrate, the formation of hillock along the scratch test and two both ends with increase of friction was not observed, as can be seen in Figure 4.22.

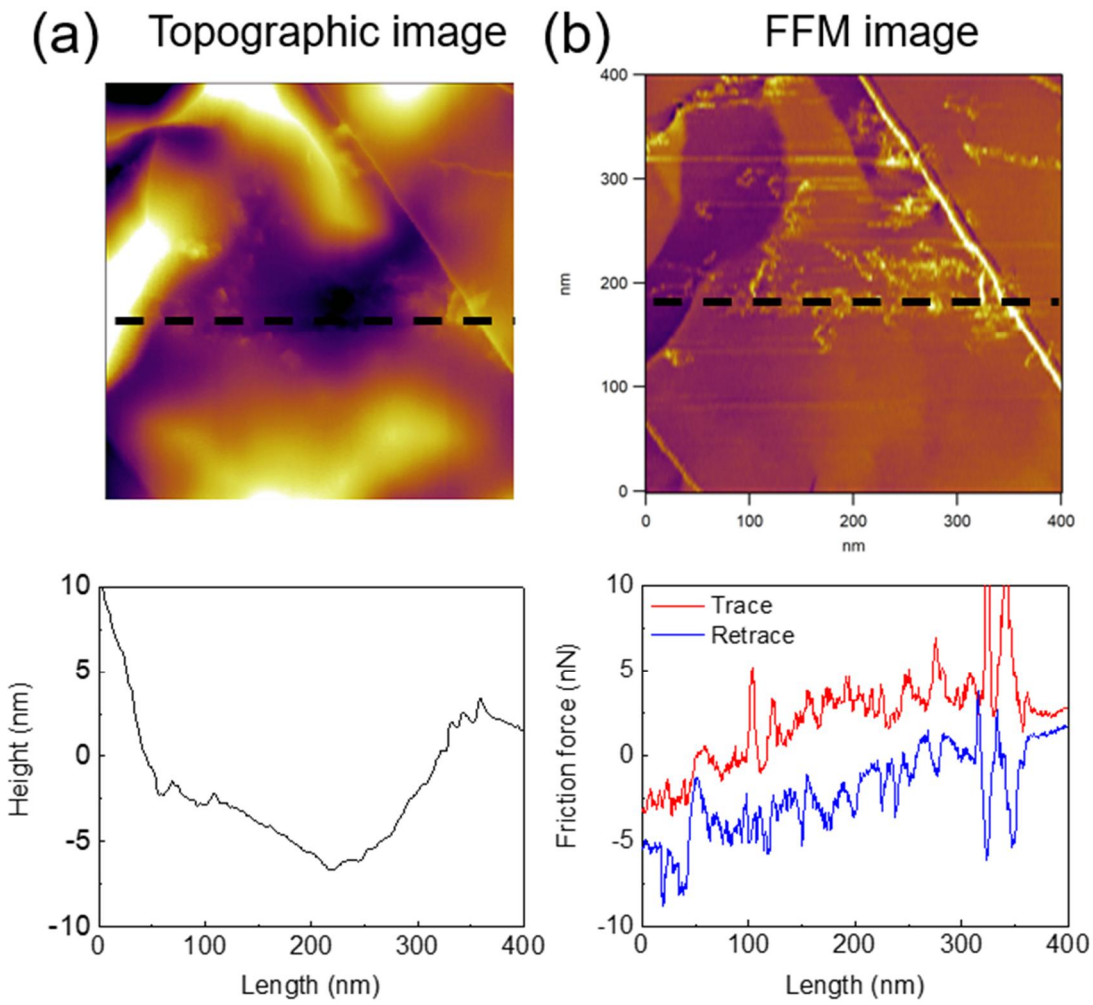

Figure 4.22 Topographic and FFM images of bi-layer graphene on CNT matrix after reciprocating scratch test.

4.3.3 Discussion

Topographic and FFM images shown the failure of bi-layer graphene on SiO_2 substrate after AFM-based reciprocating scratch test. In particular, the coating film was damaged after 12 reciprocating cycles under contact pressure as high as 21.4 GPa. The formation of the wear trach with the depth of about 0.8 nm was mainly due to the deformation of underlying substrate. In addition, the increase of friction at the wear track suggests the

failure of coating film. Furthermore, formation of hillock along the scratch and two end were observed. Na Fan et al. found that formation of hillock due to relative sliding between graphene/substrate could help to reduce friction [49]. However, it was not likely to be the case, as can be seen in Figure 4.21 (b). It may be due to the rupture of graphene at hillock area [39] which associated to repeated compressive stress during reciprocating scratch test. In addition, failure was also observed at the center of contact area due to repeated contact stress.

On the other hand, 1D/2D hybrid-structure with presence of CNTs was found to have positive influence of wear resistance. For bi-layer graphene on CNT matrix, change of friction force inside and outside was also observed. However, the damage of graphene on CNT matrix was found to be not significant compared to that of graphene on SiO_2 substrate. In particular, FFM image of graphene on CNT matrix suggest only defect was formed after reciprocating scratch test.

From topographic and FFM images, two distinct tribological behavior was observed with graphene on SiO_2 substrate and on CNT matrix. Mild damage with formation of defects suggests CNT matrix acting as nano-spring may help to reduce the contact pressure so that minimize the damage. The absence of hillock after experiment may be due to relative sliding between graphene flake and CNT and between CNTs in the matrix which associated with low adhesion properties. In particular, relative sliding could help to release compressive strain during reciprocating scratch test so that avoid the formation and rupture of pucker or hillock. Furthermore, 1D/2D hybrid-structure may help to avoid the major failure damage of graphene which associated with pucker formation. The failure damage may change from rupture of pucker to fatigue of graphene flake. The mild damage after

reciprocating scratch test could be contributed by superior fatigue strength of graphene which was reported in [61].

Chapter 5 Conclusions and recommendations

5.1 Conclusions of the research

Tribological properties of graphene on SiO_2 substrate and on CNT matrix was systematically investigated under various experimental conditions, such as orientation of CNT, thickness of CNT matrix, thickness of graphene film, and normal force. 1D/2D hybrid-structure with presence of CNT matrix shows to have better friction and wear resistant properties compared to those of graphene on SiO_2 substrate.

In particular, friction was found to be constantly smaller for graphene on CNT matrix compared with that of graphene on SiO_2 substrate regardless thickness of graphene flake or CNT matrix. This behavior could be contributed by low adhesion properties, in-plane strain of specimen during contact with AFM tip. In addition, residue in-plane strain could also contribute to low friction of specimen. Furthermore, 1D/2D hybrid-structure specimen possess heterogeneous friction properties in which friction was found to be smaller when scanning direction is parallel to axis of the fiber.

Mild damage with formation of defects was observed in topographic and FFM image of 1D/2D hybrid-structure specimen after reciprocating scratch test. CNT matrix act as nano-spring help to reduce contact pressure so that minimize surface damage of 1D/2D hybrid-structure specimen. In addition, absence of hillock and puckering formation may be contributed by low adhesion properties and relative sliding inside the structure of 1D/2D specimen. This absence could help 2D coating film avoid catastrophic damage which associated with rupture of pucker. However, due to high surface roughness, fluctuation of friction associated with topography-induce friction was observed. This behavior is expected to be minimized with uniform distribution of CNT matrix.

The findings of this work suggest the feasibility of CNT in 1D/2D hybrid-structure on improving friction and wear properties of graphene. It was expected to gain better understanding about tribological properties of 2D and 1D/2D hybrid-structure materials so that can help for the design of these materials in protective coating applications.

5.2 Recommendations for future work

Friction and wear resistance properties of graphene on SiO_2 substrate and on CNT matrix was systematically investigated in this work. Overall, the result of this work shows feasibility of 1D/2D hybrid-structure on enhance tribological properties of graphene. This result is expected to gain a better understand graphene and hybrid structure of graphene on top of CNT matrix materials so that could be helpful for better design of these material as protective coating layer. Although tribological characteristics of these specimen was carefully investigated, some interesting and challenging issues still need to be discovered for further implement of the hybrid-structure in tribological application, which will be described as below:

1. Heterogeneous friction properties of 1D/2D hybrid-structure suggest friction could be lower with horizontally aligned structure of CNT matrix. In addition, uniform distribution of CNT could be helpful to decrease fluctuation of friction which associated with topographic-induce friction effect. In addition, wilder range of contact pressure should be investigated with consideration would affect friction and wear behavior of specimen.

2. Graphene film used in this work was prepared by mechanical exfoliation method which consider as simplest method to obtain clean specimen. This method could be practical for research purpose due to small area and low efficiency. However, for further implementation of 1D/2D hybrid-structure as large scale, better approach should be considered. For example, utilization of CVD-grown graphene and other materials should be considered for 1D/2D hybrid-structure is crucial step for further investigation of these materials for implementation as solid lubricant and protective coating layer at the nano/micro scale.

REFERENCES

1. Spanu, L., S. Sorella, and G. Galli, *Nature and Strength of Interlayer Binding in Graphite.* Physical Review Letters, 2009. **103**(19): p. 196401.
2. Li, H., et al., *Superlubricity between MoS2 Monolayers.* Advanced Materials, 2017. **29**(27): p. 1701474.
3. Lin, Y. and J.W. Connell, *Advances in 2D boron nitride nanostructures: nanosheets, nanoribbons, nanomeshes, and hybrids with graphene.* Nanoscale, 2012. **4**(22): p. 6908-6939.
4. Radisavljevic, B., et al., *Single-layer MoS2 transistors.* Nature Nanotechnology, 2011. **6**(3): p. 147-150.
5. Novoselov, K.S., *Graphene: Materials in the Flatland (Nobel Lecture).* Angewandte Chemie International Edition, 2011. **50**(31): p. 6986-7002.
6. Jiang, J.-W., *Graphene versus MoS2: A short review.* Frontiers of Physics, 2015. **10**(3): p. 287-302.
7. Li, X. and H. Zhu, *Two-dimensional MoS2: Properties, preparation, and applications.* Journal of Materiomics, 2015. **1**(1): p. 33-44.
8. Falin, A., et al., *Mechanical properties of atomically thin boron nitride and the role of interlayer interactions.* Nature Communications, 2017. **8**(1): p. 15815.
9. Lee, C., et al., *Measurement of the Elastic Properties and Intrinsic Strength of Monolayer Graphene.* Science, 2008. **321**(5887): p. 385-388.
10. Bertolazzi, S., J. Brivio, and A. Kis, *Stretching and Breaking of Ultrathin MoS2.* ACS Nano, 2011. **5**(12): p. 9703-9709.

11. Tran Khac, B.-C., F.W. DelRio, and K.-H. Chung, *Interfacial Strength and Surface Damage Characteristics of Atomically Thin h-BN, MoS2, and Graphene.* ACS Applied Materials & Interfaces, 2018. **10**(10): p. 9164-9177.

12. Qi, Y., et al., *Wear Resistance Limited by Step Edge Failure: The Rise and Fall of Graphene as an Atomically Thin Lubricating Material.* ACS Applied Materials & Interfaces, 2017. **9**(1): p. 1099-1106.

13. Smijs, T., F. Galli, and A. van Asten, *Forensic potential of atomic force microscopy.* Forensic Chemistry, 2016. **2**: p. 93-104.

14. Binnig, G., C.F. Quate, and C. Gerber, *Atomic force microscope.* Physical Review Letters, 1986. **56**(9): p. 930-933.

15. Cappella, B. and G. Dietler, *Force-distance curves by atomic force microscopy.* Surface Science Reports, 1999. **34**(1–3): p. 1-104.

16. Mate, C.M., et al., *Atomic-scale friction of a tungsten tip on a graphite surface.* Phys.Rev.Lett., 1987. **59**(17): p. 1942-1945.

17. Cappella, B., *Mechanical Properties of Polymers Measured through AFM Force-Distance Curves*. 2016: Springer International Publishing.

18. Sahin, O., et al., *An atomic force microscope tip designed to measure time-varying nanomechanical forces.* Nature Nanotechnology, 2007. **2**(8): p. 507-514.

19. Rabe, U. and W. Arnold, *Acoustic microscopy by atomic force microscopy.* Applied Physics Letters, 1994. **64**(12): p. 1493-1495.

20. Sundararajan, S. and B. Bhushan, *Topography-induced contributions to friction forces measured using an atomic force/friction force microscope.* Journal of Applied Physics, 2000. **88**(8): p. 4825-4831.

21. Tran-Khac, B.-C., et al., *Operational and environmental conditions regulate the frictional behavior of two-dimensional materials.* Applied Surface Science, 2019. **483**: p. 34-44.

22. Hutter, J.L. and J. Bechhoefer, *Calibration of atomic□force microscope tips.* Review of Scientific Instruments, 1993. **64**(7): p. 1868-1873.

23. Varenberg, M., I. Etsion, and G. Halperin, *An improved wedge calibration method for lateral force in atomic force microscopy.* Review of Scientific Instruments, 2003. **74**(7): p. 3362-3367.

24. Holmberg, K., P. Andersson, and A. Erdemir, *Global energy consumption due to friction in passenger cars.* Tribology International, 2012. **47**: p. 221-234.

25. Nine, M.J., et al., *Graphene: a multipurpose material for protective coatings.* Journal of Materials Chemistry A, 2015. **3**(24): p. 12580-12602.

26. Chung, Y.-W., *Micro- and Nanoscale Phenomena in Tribology*. 2011.

27. Schumacher, A., et al., *Influence of humidity on friction measurements of supported MoS2 single layers.* Journal of Vacuum Science & Technology B: Microelectronics and Nanometer Structures Processing, Measurement, and Phenomena, 1996. **14**(2): p. 1264-1267.

28. Xu, M., et al., *Lithium-assisted exfoliation of pristine graphite for few-layer graphene nanosheets.* Nano Research, 2015. **8**(3): p. 801-807.

29. Hernandez, Y., et al., *High-yield production of graphene by liquid-phase exfoliation of graphite.* Nature Nanotechnology, 2008. **3**(9): p. 563-568.

30. Zhou, K.-G., et al., *A Mixed-Solvent Strategy for Efficient Exfoliation of Inorganic Graphene Analogues.* Angewandte Chemie International Edition, 2011. **50**(46): p. 10839-10842.

31. Vasić, B., et al., *Nanoscale wear of graphene and wear protection by graphene.* Carbon, 2017. **120**: p. 137-144.

32. Berman, D., et al., *Extraordinary Macroscale Wear Resistance of One Atom Thick Graphene Layer.* Advanced Functional Materials, 2014. **24**(42): p. 6640-6646.

33. Shin, Y.J., et al., *Frictional characteristics of exfoliated and epitaxial graphene.* Carbon, 2011. **49**(12): p. 4070-4073.

34. Marchetto, D., et al., *Friction and Wear on Single-Layer Epitaxial Graphene in Multi-Asperity Contacts.* Tribology Letters, 2012. **48**(1): p. 77-82.

35. Kim, K.-S., et al., *Chemical Vapor Deposition-Grown Graphene: The Thinnest Solid Lubricant.* ACS Nano, 2011. **5**(6): p. 5107-5114.

36. Won, M.-S., O.V. Penkov, and D.-E. Kim, *Durability and degradation mechanism of graphene coatings deposited on Cu substrates under dry contact sliding.* Carbon, 2013. **54**: p. 472-481.

37. Berman, D., A. Erdemir, and A.V. Sumant, *Few layer graphene to reduce wear and friction on sliding steel surfaces.* Carbon, 2013. **54**: p. 454-459.

38. Wählisch, F., et al., *Friction and atomic-layer-scale wear of graphitic lubricants on SiC(0001) in dry sliding.* Wear, 2013. **300**(1): p. 78-81.

39. Klemenz, A., et al., *Atomic Scale Mechanisms of Friction Reduction and Wear Protection by Graphene.* Nano Letters, 2014. **14**(12): p. 7145-7152.

40. Zandiatashbar, A., et al., *Effect of defects on the intrinsic strength and stiffness of graphene.* Nat Commun, 2014. **5**(- 1): p. 3186.

41. Gomez-Navarro, C., M. Burghard, and K. Kern, *Elastic properties of chemically derived single graphene sheets.* Nano Lett, 2008. **8**(7): p. 2045-9.

42. Zhang, P., et al., *Fracture toughness of graphene.* Nat Commun, 2014. **5**(- 1): p. 3782.

43. Santos, E.J.G., et al., *Magnetism of Single Vacancies in Rippled Graphene.* Journal of Physical Chemistry C, 2012. **116**(13): p. 7602-7606.

44. Shekhawat, A. and R.O. Ritchie, *Toughness and strength of nanocrystalline graphene.* Nat Commun, 2016. **7**(- 1): p. 10546.

45. Ferrari, A.C., et al., *Science and technology roadmap for graphene, related two-dimensional crystals, and hybrid systems.* Nanoscale, 2015. **7**(11): p. 4598-4810.

46. Cameron, J.S., et al., *Accurate thickness measurement of graphene.* Nanotechnology, 2016. **27**(12): p. 125704.

47. Li, J., et al., *Molecular Origin of Superlubricity between Graphene and a Highly Hydrophobic Surface in Water.* The Journal of Physical Chemistry Letters, 2019. **10**(11): p. 2978-2984.

48. Berman, D., et al., *Macroscale superlubricity enabled by graphene nanoscroll formation.* Science, 2015. **348**(6239): p. 1118-1122.

49. Fan, N., et al., *A hillock-like phenomenon with low friction and adhesion on a graphene surface induced by relative sliding at the interface of graphene and the SiO2 substrate using an AFM tip.* Nanoscale Advances, 2020. **2**(6): p. 2548-2557.

50. Zhang, S., et al., *Tuning friction to a superlubric state via in-plane straining.* Proceedings of the National Academy of Sciences, 2019. **116**(49): p. 24452-24456.

51. Tran Khac, B.C. and K.-H. Chung, *Quantitative assessment of contact and non-contact lateral force calibration methods for atomic force microscopy.* Ultramicroscopy, 2016. **161**: p. 41-50.

52. Chung, K.-H. and M.G. Reitsma, *Note: Lateral force microscope calibration using multiple location pivot loading of rectangular cantilevers.* Review of Scientific Instruments, 2010. **81**(2): p. 026104.

53. Kumar, A., T. Staedler, and X. Jiang, *Effect of normal load and roughness on the nanoscale friction coefficient in the elastic and plastic contact regime.* Beilstein Journal of Nanotechnology, 2013. **4**: p. 66-71.

54. Li, Q., et al., *Substrate effect on thickness-dependent friction on graphene.* physica status solidi (b), 2010. **247**(11-12): p. 2909-2914.

55. Lucas, M., et al., *Hindered rolling and friction anisotropy in supported carbon nanotubes.* Nature Materials, 2009. **8**(11): p. 876-881.

56. McFarlane, J.S., D. Tabor, and F.P. Bowden, *Relation between friction and adhesion.* Proceedings of the Royal Society of London. Series A. Mathematical and Physical Sciences, 1950. **202**(1069): p. 244-253.

57. Liu, S.-W., et al., *Robust microscale superlubricity under high contact pressure enabled by graphene-coated microsphere.* Nature Communications, 2017. **8**(1): p. 14029.

58. Brazhkin, V.V., A.G. Lyapin, and R.J. Hemley, *Harder than diamond: Dreams and reality.* Philosophical Magazine A, 2002. **82**(2): p. 231-253.

59. Lee, J.-U., D. Yoon, and H. Cheong, *Estimation of Young's Modulus of Graphene by Raman Spectroscopy.* Nano Letters, 2012. **12**(9): p. 4444-4448.

60. Tran, T.V. and K.-H. Chung, *Tribological Characteristics of Single-Layer h-BN Measured by Colloidal Probe Atomic Force Microscopy.* Coatings, 2020. **10**(6).

61. Cui, T., et al., *Fatigue of graphene.* Nature Materials, 2020. **19**(4): p. 405-411.